Journal Pre-proof

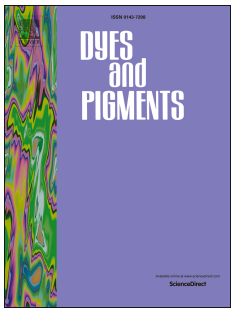

Donor-acceptor architectures of tetraphenylethene linked aza-BODIPYs: Synthesis, crystal structure, energy transfer and computational studies

Naresh Balsukuri, Neha Manav, Mohsin Y. Lone, Shigeki Mori, Aritra Das, Pratik Sen, Iti Gupta

PII: S0143-7208(19)32844-X

DOI: https://doi.org/10.1016/j.dyepig.2020.108249

Reference: DYPI 108249

To appear in: *Dyes and Pigments*

Received Date: 4 December 2019

Revised Date: 22 January 2020

Accepted Date: 26 January 2020

Please cite this article as: Balsukuri N, Manav N, Lone MY, Mori S, Das A, Sen P, Gupta I, Donor-acceptor architectures of tetraphenylethene linked aza-BODIPYs: Synthesis, crystal structure, energy transfer and computational studies, *Dyes and Pigments* (2020), doi: https://doi.org/10.1016/j.dyepig.2020.108249.

Manuscript Title:

Donor-Acceptor architectures of tetraphenylethene linked aza-BODIPYs: Synthesis, crystal structure, energy transfer and computational studies

Graphical Abstract

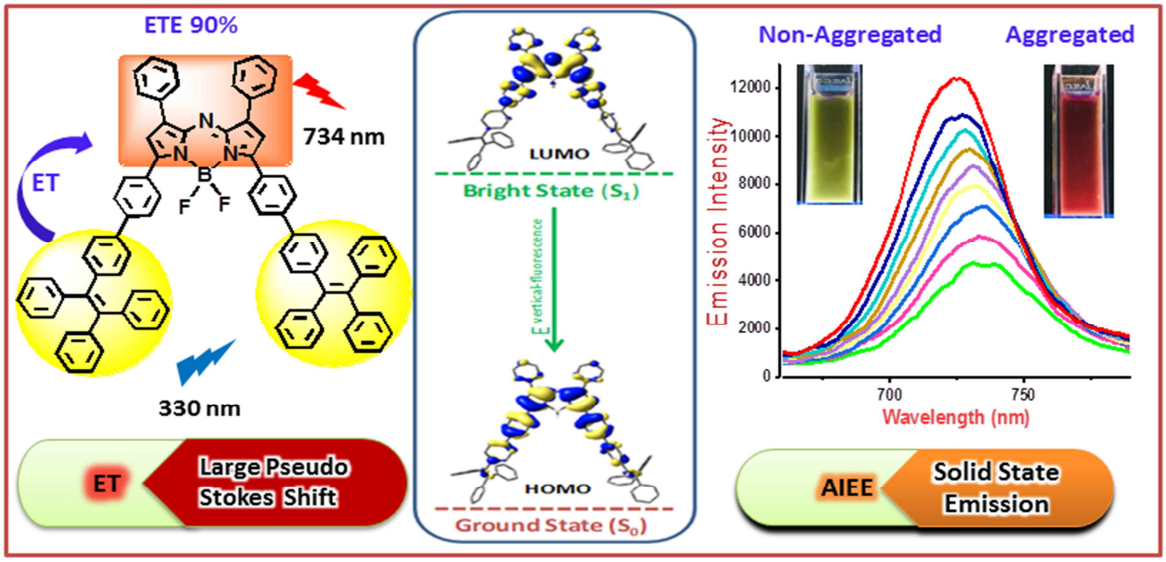

Donor-Acceptor architectures of tetraphenylethene linked aza-BODIPYs: Synthesis, crystal structure, energy transfer and computational studies

Naresh Balsukuri,[a] Neha Manav,[a] Mohsin Y. Lone,[a] Shigeki Mori,[b] Aritra Das,[c] Pratik Sen,[c] and Iti Gupta*[a]

[a]Indian Institute of Technology Gandhinagar, Palaj Campus, Gandhinagar, Gujarat- 382355, India
[b]Advanced Research Support Center, Ehime University, Matsuyama 790-8577, Japan
[c] Department of Chemistry, Indian Institute of Technology Kanpur, Uttar Pradesh-208016, India
*Corresponding author, e-mail: iti@iitgn.ac.in

Abstract

This work is focused on the design and synthesis of donor-acceptor pairs comprising of aza-BODIPY and tetraphenylethene (TPE) fluorogens with large pseudo Stokes shifts (386 to 424 nm). Femtosecond transient absorption spectroscopy, single crystal X-ray technique and TD-DFT studies were used to get more insight about their spectral behavior. As compared to the tetra-phenylaza-BODIPY, the four aza-BODIPYs exhibited 50-90 nm red shifted absoprtion and emission spectra. When the donor-acceptor architectures were excited at 300 nm, the aza-BODIPY unit emitted strong fluorescence in red region. This suggested an intramolecular energy transfer between donor (TPE) and the aza-BODIPY acceptor; with 81-90% energy transfer efficiencies. Femtosecond transient absorption studies also supported energy transfer process in the molecules, with 3.7 ps time constant associated with it. Aggregation studies in THF/n-heptane solution showed hypsochromic shifts in the aggregated form; X-ray packing structures indicated H-type aggregates (slip angle > 54.7^{o}) in the solid state. Scanning electron microscopy (SEM) measurement revealed 200-700 nm size sphere shaped structures in the aggregated forms.

Keywords: Aza-BODIPY, Donor-Acceptor System, Aggregation studies, Energy transfer, pseudo Stokes shifts, TD-DFT, Transient absorption.

Introduction

The π-conjugated organic NIR (near infra-red) fluorescent dyes have gained much attention due to their highly varied applications, ranging from chemosensors, bio-markers, as photosensitizers in DSSCs (Dye Sensitized Solar Cells) and in OLEDs (Organic Light Emitting Diodes) as electroluminescent materials [1-4]. As NIR light causes minimal photo-damage and can penetrate deep into biological tissue, thus NIR dyes can be used as contrast agents in bioimaging [5]. Among the numerous fluorescent dyes, the BODIPY (BF_2-chelated dipyrromethenes) is one of the most extensively studied fluorophore with wide applications in toxic metal sensing, optoelectronic materials, fluorescent tags, photovoltaics and light harvesting antenna systems [6-10]. The BODIPYs have excellent photochemical stability, large absorption coefficients, amenable to structural modifications and narrow emission spectra with high quantum yields [11,12]. In aggregated state, BODIPYs show reduced fluorescence and minor Stokes Shifts (10-25 nm) due to aggregation-caused quenching (ACQ); which limits their applications [13]. On the other hand, the propeller shape molecules viz. hexaphenylsilole (HPS) and tetraphenylethyene (TPE) exhibit strong fluorescence upon aggregation; due to the restriction of intramolecular motions (RIM) which reduces the non-radiative decay processes. This phenomenon is known aggregation induced emission (AIE) and was first reported by Tang and coworkers [14,15]. The TPE derivatives show good chemical stability and can be easily functionalized; their AIE property can be exploited to prepare fluorescent probes for biomolecules and explosives [16-18]. Tang and coworkers demonstrated that, a typical ACQ fluorophore when linked to the HPS or TPE molecules; it can produce novel fluorogens with enhanced fluorescence properties [19]. The BODIPYs substituted with TPE have exhibited large Stokes shifts and tunable emission properties [20]. When the *meso*-carbon of the dipyrromethene core of the BODIPY is exchanged

by a nitrogen atom, the resultant molecule is called an Aza-BODIPY [21-24]. Aza-BODIPYs absorbs and emits in the NIR (near infra-red) region (650-900 nm) and they also suffer from ACQ effect; however owing to their strong absorption in biological window they are ideal candidates for photodynamic therapy, deep tissue imaging and energy transfer systems [25,26].

Fluorescence resonance energy transfer (FRET) process can be used to adjust the optical and electronic properties of donor-acceptor (D-A) systems including BODIPYs and Aza-BODIPYs [27-32]. The efficiency of energy transfer in FRET based systems may vary depending on the D-A distance, their relative orientation and also on the spectral overlap between the D emission and A absorption [33-39]. Particularly, in BODIPY based D-A designs [40-42] employing a D with high emission quantum yield leads to leakage of fluorescence from the D; this drawback may restrict their application in biology. Recent report on dark resonance energy transfer (DRET) based BODIPYs by Chang and coworkers [43], demonstrated a complementary approach where a non-fluorescent molecules is used as “dark donor”. The use of TPE in D-A based molecular designs reduces fluorescence leakage from the D; as a result the energy transfer efficiency is relatively higher than FRET based systems [44]. Furthermore, the large pseudo Stokes shifts and emission shifts rule out the fluorescence detection errors and possibility of self-quenching [44,45]. The AIE active fluorophore like TPE can be linked to aza-BODIPY to demonstrate energy transfer phenomenon in NIR region; and NIR dyes can be designed for biological applications and solar energy systems. With this intention, we have designed four novel AIE fluorogens comprising of TPE and NIR aza-BODIPYs. Herein we present, the synthesis, X-ray structure, optical, aggregation induced enhanced emission (AIEE) and electrochemical studies of NIR aza-BODIPYs. The 1,7-positions of the aza-BODIPY core

were substituted by 2-thienyl, phenyl and *N*-butylcarbazole rings; whereas 3,5-phenyl rings were linked with TPE groups at their *para*-positions (Chart 1).

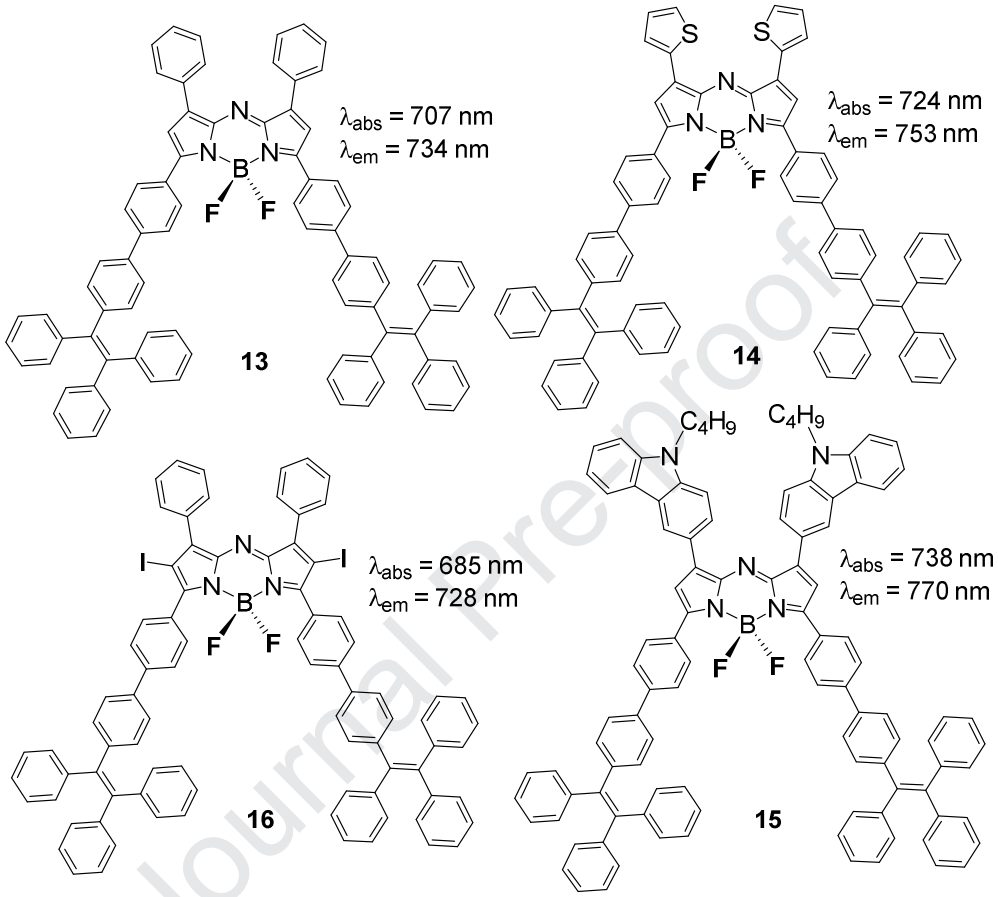

Chart 1. TPE substituted aza-BODIPYs **13-16** reported in this work (data recorded in toluene).

All four aza-BODIPYs exhibit considerable red shifs (50-90 nm) in their absoprtion and emission maxima w.r.t. the parent tetraphenyl aza-BODIPY. The fluorescence studies in THF (tetrahydrofuran)/ heptane mixture were investigated by varying the n-heptane content ($f_h \geq$ 10-90%). The molecular packing diagram obtained from X-ray crystal structure, solid state absorption, emission and singlet oxygen generation studies were also reported for the selected aza-BODIPYs. To the best of our knowledge this is the first report, where TPE substituted NIR aza-BODIPYs are exhibiting considerably large pseudo Stokes shifts due to energy transfer. In

addition, DFT and TD-DFT calculations were performed to acquire the spectroscopic insight of absorption and emission properties of the aza-BODIPYs reported here.

Results and Discussion

Synthesis and Characterization

The synthetic protocol to prepare aza-BODIPYs **13-15** is shown in schemes 1 and 2. The synthesis of aza-BODIPYs was carried out in four steps; which involve preparation of chalcones, nitrochalcones, aza-dipyrromethenes and aza-BODIPYs [46].

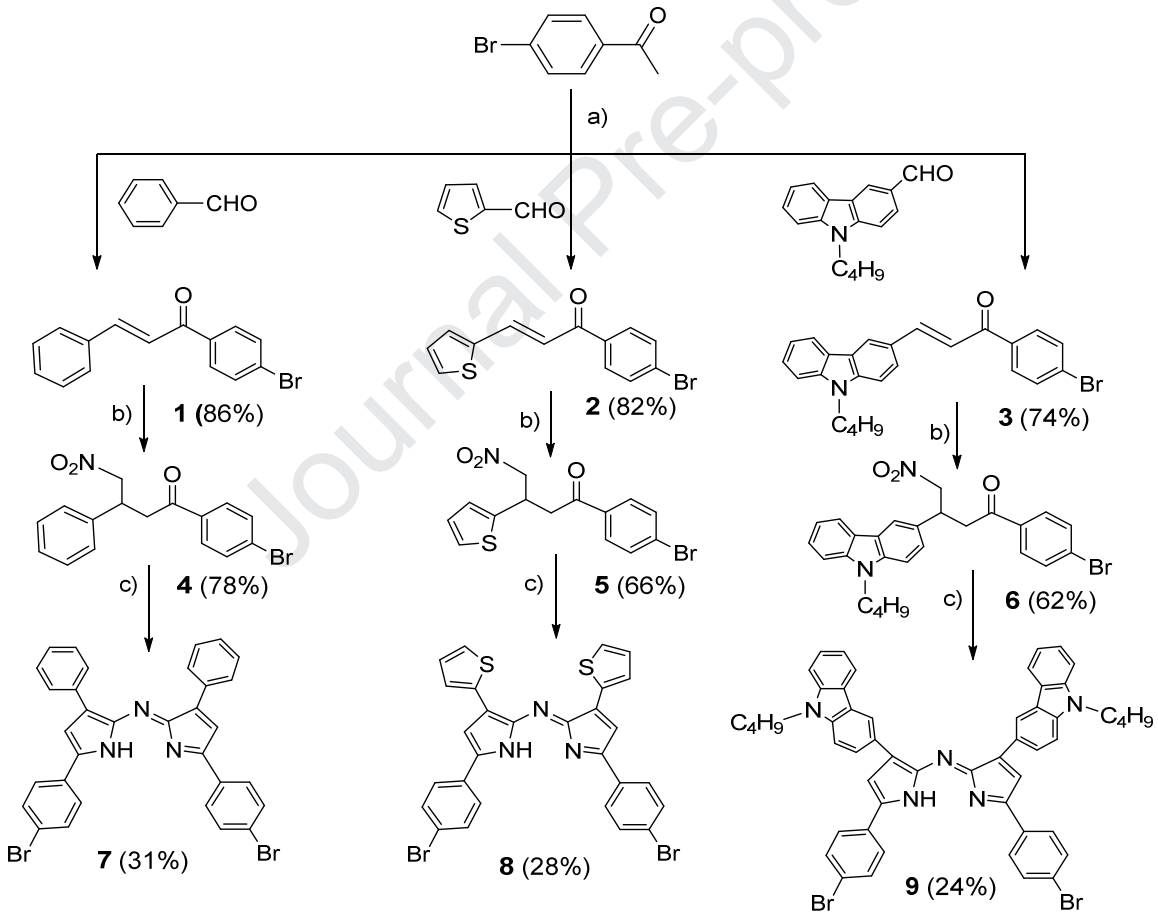

Scheme 1. Synthetic route for aza-dipyrromethenes **7-9**. a) NaOH, Grinding method; b) KOH, CH_3NO_2, EtOH, reflux 12 h; c) NH_4OAc, EtOH, reflux 24 h.

The chalones **1-3** were prepared by aldol condensation reaction between 4-bromoacetophenone and the corresponding aldehydes (Scheme 1). The compounds **1-3** were formed as yellow coloured solids in 57-66% yields. Next, 1,4-Michael addition was carried out between chalcones **1-3** and nitromethane in the presence of base KOH in ethanol; the pure nitrochalcones **4-6** were obtained as the oily compounds in 50-70% yield after silica gel chromatography.

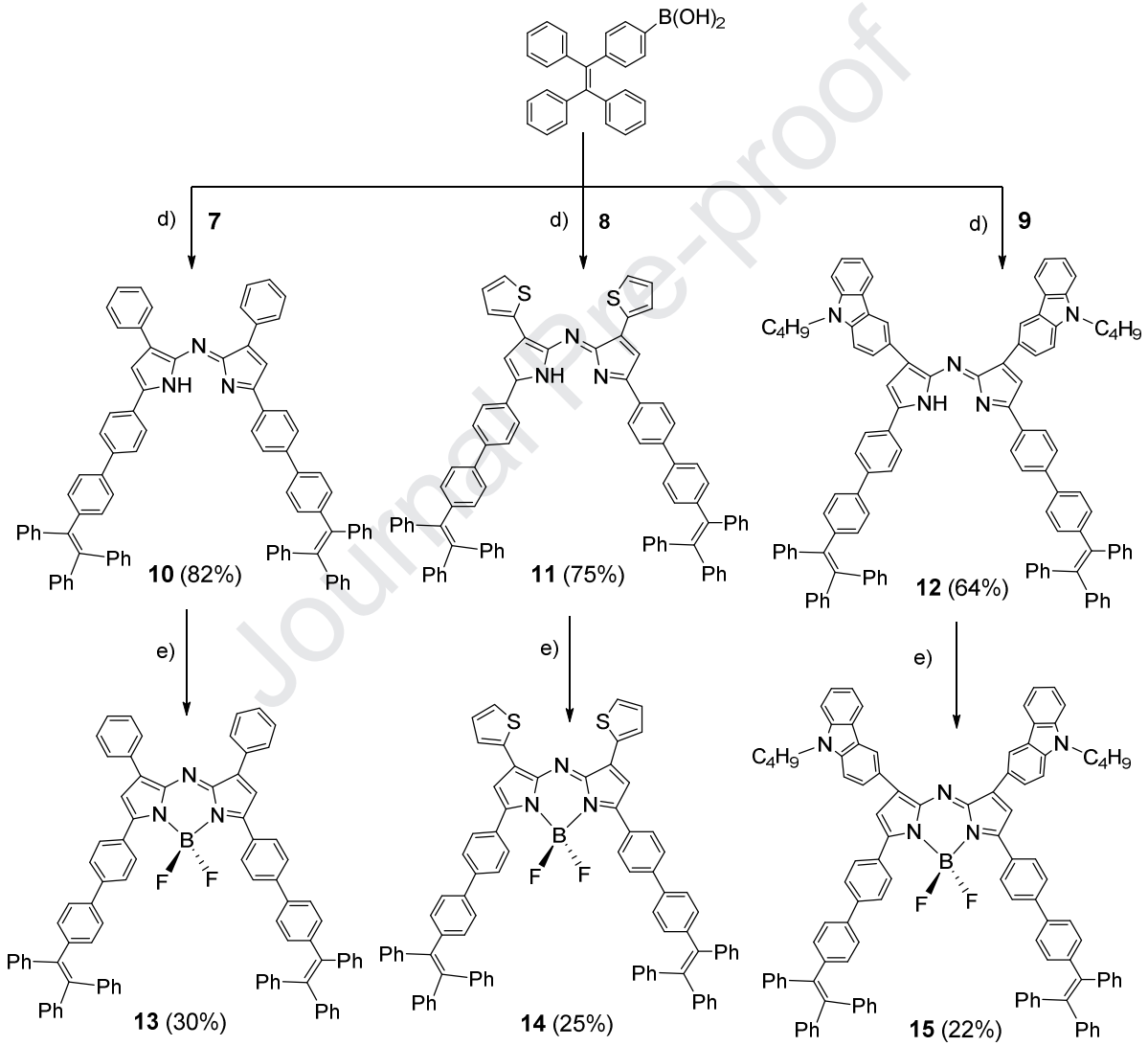

Scheme 2. Synthetic route for aza-BODIPYs **13-15**. d) $Pd(PPh_3)_4$, toluene/THF, EtOH, K_2CO_3; e) $BF_3.OEt_2$, CH_2Cl_2/ NEt_3, rt, 24 h.

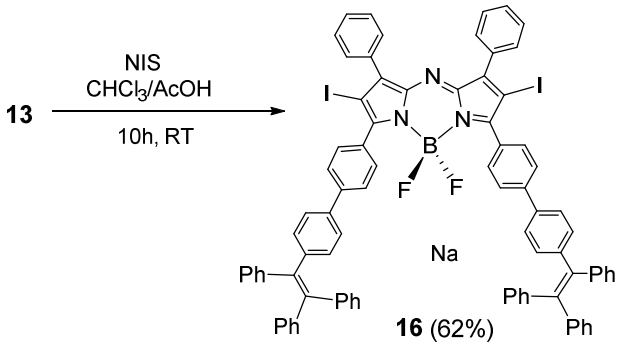

Scheme 3. Synthesis of aza-BODIPY **16**.

Then compounds **4-6** were reacted with ammonium acetate in ethanol to form aza-dipyrromethenes **7-9** as blue colour precipitate; washing with cold ethanol gave pure **7-9** in 16-20% yields (Scheme 1). After preparing the aza-BODIPYs framework next step was to attached energy donor groups (TPE) and it was achieved by Suzuki-Miyaura coupling of **7-9** with TPE-$B(OH)_2$ [47]. The TPE-$B(OH)_2$ was synthesized as per the reported procedure [47]. Compounds **7-9** were refluxed (Scheme 2) with TPE-$B(OH)_2$ in the prescence of palladium catalyst $Pd(PPh_3)_4$ and K_2CO_3 base for 24 h. The coupling of TPE-$B(OH)_2$ with compounds **7-9** was checked by TLC (thin layer chromatography) and the observation of new blue green spot on TLC indicated formation of the desired product. The TPE substituted aza-dipyrromethenes **10-12** were relatively unstable and crude reaction mixture was directly used for the synthesis of aza-BODIPYs. The aza-BODIPYs **13-15** were formed as dark brown (**13**) and blue colour (**14** and **15**) compounds when aza-DPMs **10-12** were reacted with BF_3OEt_2 for 24 h. The pure aza-BODIPYs **13-15** were obtained in 38-46% yields after silica gel column chromatography. In order to make triplet photosensitizer based on aza-BODIPY, the iodo substituents were linked at the β-pyrrole position of aza-BODIPY.

In this regard, diiodo- substituted aza-BODIPY **16** was synthesized by treating aza-BODIPY **15** with *N*-iodosuccinimide (Scheme 3) for 10 h to get product in 62% yield. All the compounds were characterized by ^{1}H, ^{13}C NMR, ESI- or MALDI-MS spectrometry (Supplementary Information). The ^{19}F and ^{11}B NMR also confirmed the formation of aza-BODIPYs **13-16**. In aza-BODIPY **13-16**, the coupling of two fluorine atoms with the adjacent boron atom (I = 3/2) caused ^{19}F signal split into quartet. Simultaneously boron atom showed up as triplet attributed to coupling with fluorine atom (I = 1/2). For aza-BODIPYs **13-16** the ^{19}F signals were appeared arround -130.36 to -131.40 ppm; and the ^{11}B signals were observed between 0.92 to 1.16 ppm (Supplementary Information).

X-ray Crystal Studies

The single crystal suitable for X-ray diffractions was developed by slow evaporation of the solution of aza-BODIPY **13** (CCDC 1814178) in chloroform/n-heptane solvent mixture. The crystal structure of aza-BODIPY **13** appeared as green block crystal with triclinic system having P-1(#2) space group. The X-ray structure and packing diagram with intramolecular interactions are shown in figures 1 and 2, respectively. X-ray crystal structure parameters are provided in the supplementary information (Tables S1, S2). The four phenyl rings of two TPE units are arranged in propeller shape conformation due to steric bulkiness. Noticeably, the aza-dipyrrin core is perpendicular to the two TPE units (Figure 2a). The dihedral angles between aza-dipyrrin plane and one of the lower phenyl rings linked to TPE unit were quite small [C7-C8-C53-C54, 2.2(6)^{o} and N3-C8-C53-C58, 1.1(7)^{o}]; which made the lower phenyl ring almost coplanar to the aza-dipyrrin core. The torsion angles [C1-C2-C9-C10, N1-C1-C9-C14] between the other lower phenyl ring and aza-dipyrrin plane are 29.6(6)^{o} and 30.1(7)^{o}, respectively.

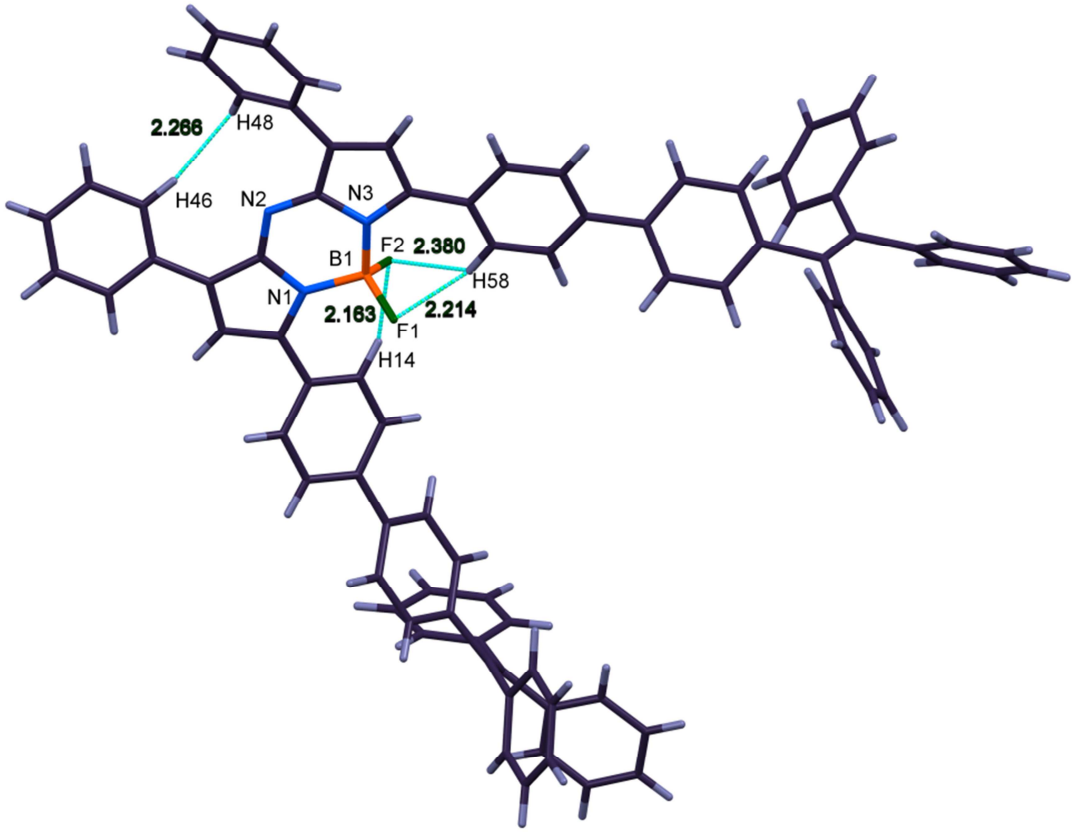

Figure 1. X-ray structure of aza-BODIPY **13,** dotted colorized lines stand for weak intramolecular interactions.

Also, the torsion angles [C12-C13-C15-C20, C57-C56-C59-C60] between the lower phenyl rings and the phenyl ring of TPE are 26.6(6)^{o} and 29.8(6)^{o}, respectively. These smaller dihedral angles indicated enhanced electronic communication between the aza-dipyrrin core and the TPE units in compound **13**. The packing diagram of **13** obtained from X-ray crystal structure, revealed slipped stack arrangements of aza-dipyrrin planes of two adjacent molecules (Figure 2a) with significant π–π interactions. The solid state packing diagram of **13** and the orientation of the transition dipoles relative to the stacking axis can be helpful to explain the type of aggregates [48]. The center to center distances between these aza-dipyrrin cores are 4.55 and 6.08 Å and the ground state dipole moment (0.88 D) of **13,** was aligned with $N_{meso} \rightarrow$ B vector which has antiparallel alignment in the columnar stacks (Figure 2b). The two aza-dipyrrin units of neighboring

molecules were parallel to each other and the interplanar separation of the mean planes of the adjacent molecules was of 3.94 Å.

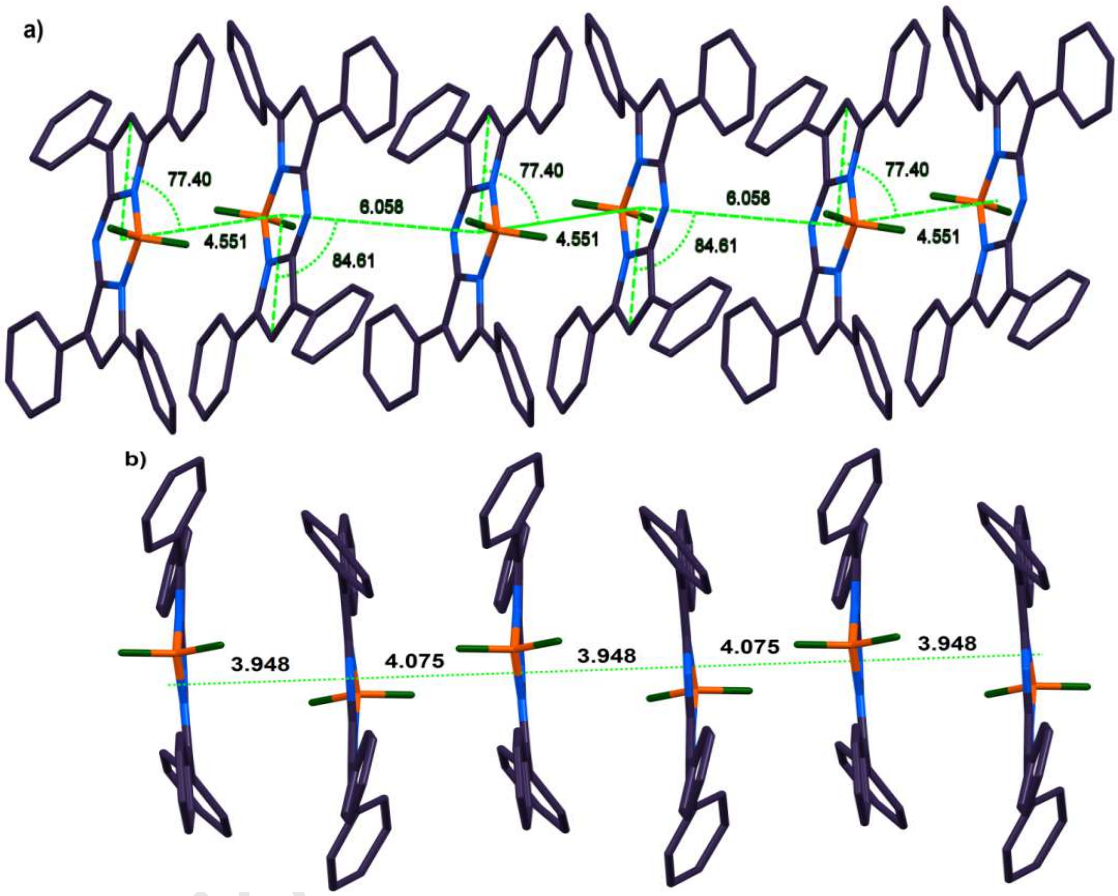

Figure 2. (a) Packing diagram of **13**, displaying center to center distances and slip angle; (b) Distances of the mean planes of adjacent molecules, H atoms and TPE units are omitted for clarity.

Thus, aza-BODIPY **13** displayed intermolecular slipped π–π stacking in the crystal state with slip angle of 77.04^{o} (Figure 2a). According to Kasha's molecular exciton model [49], the H-type aggregates are non-fluorescent due to forbidden nature of the lowest excited state in the aggregates. Exceptionally, emission from H-type aggregates is observed when forbidden nature of the excited state is reduced due to minor deviations of the direction of the transition dipoles between adjacent neighbours [50]. When the molecules possess inclined geometry in the

aggregated state, the transition dipoles would not be cancelled out, therefore fluorescence is not completely quenched from H-type aggregates. This could be the probable reason of the observed

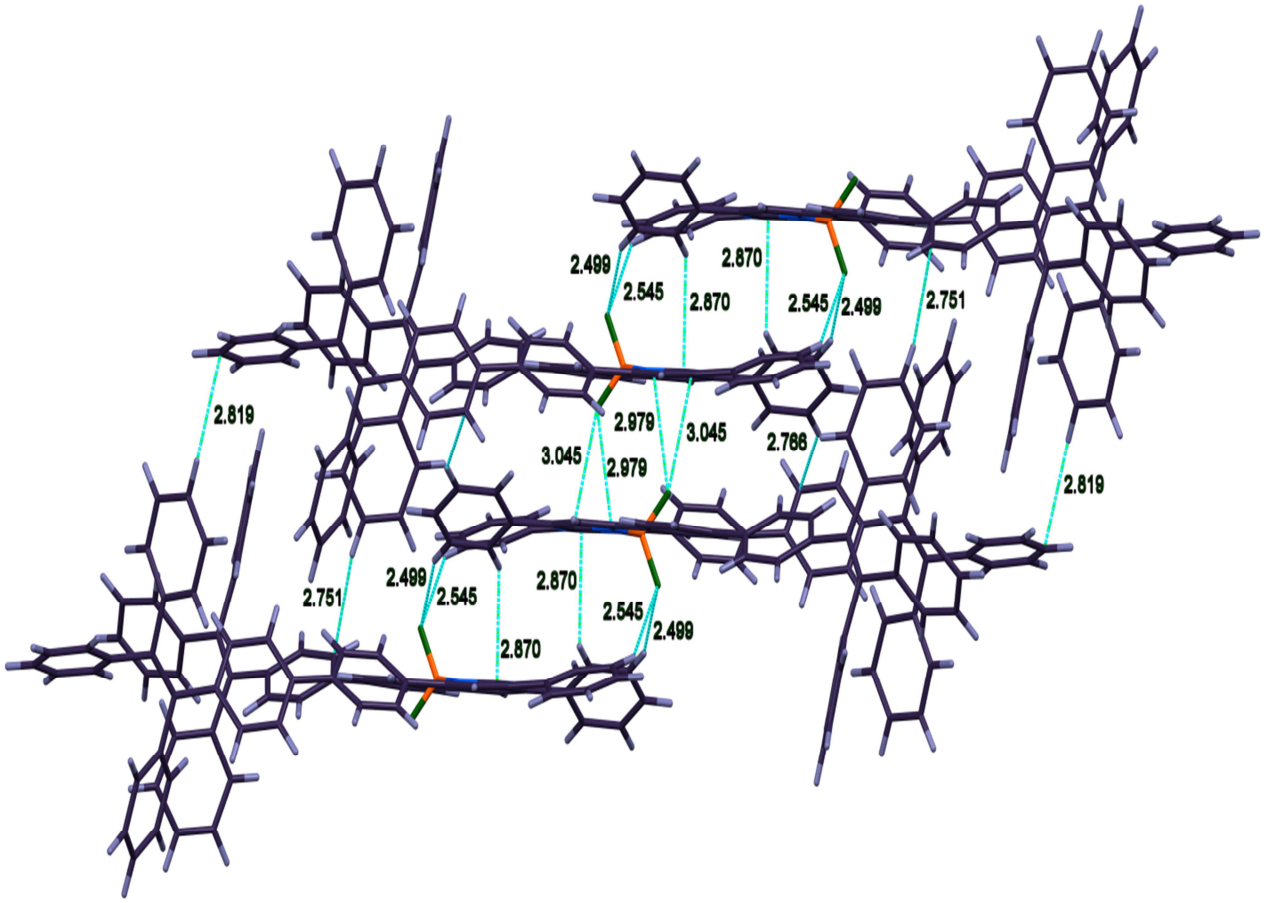

Figure 3. Molecular packing diagram of aza-BODIPY **13** with inter-molecular interactions.

fluorescence from aggregated state of aza-BODIPY **13**; which exhibited H-type aggregates with slip angle $\theta > 54.7^{o}$ in the packing diagram (Figure 2a). Also, hypsochromic shift in the fluorescence emission during aggregation studies indicated H-type aggregates in solution. Furthermore, intermolecular H-bonding (B-F-----H) interactions (Table S3) as evident in crystal packing diagram, are likely to favor the parallel slipped π–π stacking of molecules in solid state (Figure 3).

Absorption and Emission Properties

The experimentally determined photophysical properties of aza-BODIPYs **13-16** are presented in table 1. A comparison of absorption spectra of compounds **13-16** is shown in figure 4a, an intense band between 600-820 nm (ε = 42,600-79,500 $M^{-1}cm^{-1}$) corresponds to $S_o \rightarrow S_1$ transitions and another band around 500-600 nm with medium intensity (ε = 14,500-45,500 $M^{-1}cm^{-1}$) was assigned to $S_o \rightarrow S_2$ transitions originating from the aza-BODIPY core [21]. Additional absorption band at ~340 nm of moderate intensity (ε = 46,500-89,000 $M^{-1}cm^{-1}$) was assigned to the two TPE units attached on aza-BODIPYs [44]. The major absorption band of compounds **13-16** was moved to NIR region, depending upon the nature of substituents present at 1,7- and 3,5-positions of the aza-BODIPY chromophore. Change of the substituents from phenyl (**13**) to thiophene (**14**) at 1,7-positions of aza-BODIPY, led to bathochromic shift of 17 nm in the absorption maximum of **14**. The bathochromic shift in **14** can be ascribed to the smaller ring size of thiophene, making the electron rich heterocycle more coplanar with the aza-BODIPY plane.

Table 1. Absorption and emission data of compounds **13-16** in various solvents.

Compound	Solvent	λ_{ab} (nm), ε (log E)	λ_{em} (nm)	Φ_f[a]	Stokes shift (nm)	(cm^{-1})
13	Toluene	707 (4.82), 510 (4.16), 348 (4.67)	734	0.42	27	520
	Chloroform	703 (4.69), 509 (4.09), 345 (4.56)	734	0.38	31	600
	Tetrahydrofuran	705 (4.63), 505 (4.00), 345 (4.51)	736	0.19	31	597
14	Toluene	724 (4.90), 537 (4.29), 344 (4.78)	753	0.18	29	531
	Chloroform	722 (4.87), 545 (4.23), 342 (4.72)	754	0.15	32	587
	Tetrahydrofuran	721 (4.80), 543 (4.19), 342 (4.68)	753	0.10	32	589
15	Toluene	738 (4.92), 604 (4.66), 344 (4.95)	770	0.09	32	563
	Chloroform	738 (4.87), 614 (4.69), 343 (4.97)	782	0.07	44	762
	Tetrahydrofuran	741 (4.82), 621 (4.65), 342 (4.91)	790	0.05	49	837
16	Toluene	685 (4.93), 520 (4.31), 325 (4.78)	728	0.02	43	862
	Chloroform	680 (4.84), 519 (4.23), 329 (4.69)	729	0.02	49	988
	Tetrahydrofuran	679 (4.71), 512 (4.13), 329 (4.57)	727	0.01	52	1047

a: 1,7-dinaphthyl-3,5-dithienyl azaBODIPY (Φ_f = 0.14, $CHCl_3$) used as standard, λ_{ex} = 650 nm.

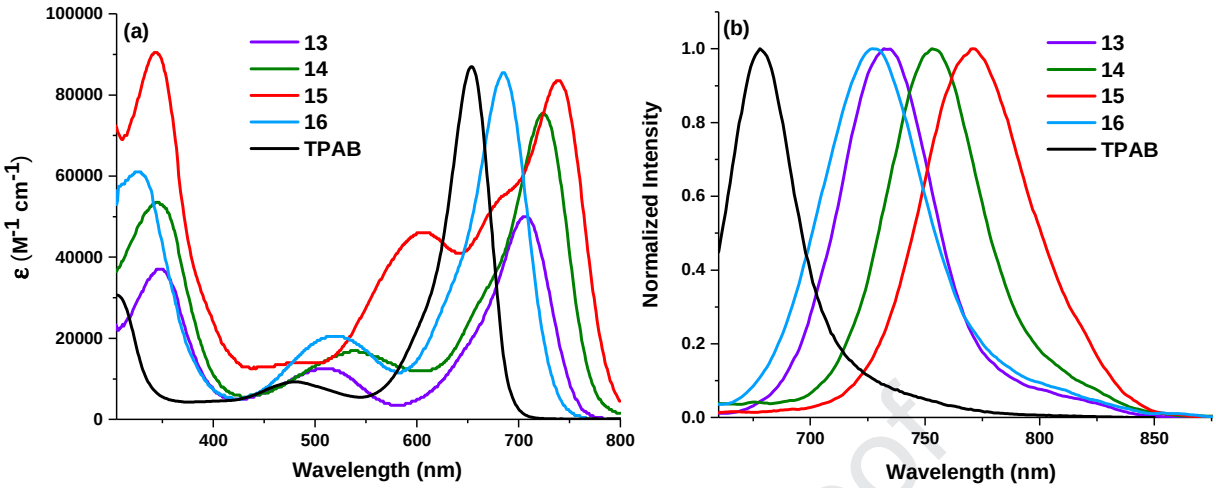

Figure 4. Comparison of (a) absorption and (b) emission spectra of aza-BODIPYs **TPAB**, **13-16**, recorded in toluene (λ_{ex} = 650 nm).

Furthermore, due to the presence of strong electron donor aromatic ring like *N*-butylcarbazole, compound **15** showed significantly red shifted (31 nm) absorption in solution. Remarkably, the absorption of **13** was 57 nm red shifted as compared to parent tetraphenyl aza-BODIPY (TPAB, λ_{abs} = 650) [51]. It may be due to the extended π conjugation of TPE units present on the 3,5-phenyls in the compound. Noticeably, as compared to TPAB the major absorption bands of **14** and **15** were red shifted by 74 and 88 nm, respectively. The major absorption band of 2,6-diiodo substituted aza-BODIPY **16** was 35 nm red shifted as compared to the TPAB. The fluorescence spectra of aza-BODIPYs **13-16** are shown in figure 4(b) and emission quantum yields are given in table 1. All aza-BODIPYs **13-16** displayed intense emission maxima in the range of 734-770 nm due to $S_1 \rightarrow S_0$ transitions (Figure 4b). The emission maxima of **13-16** were substantially red shifted (Table 1) as compared to the parent TPAB emission (λ_{em} = 672 in $CHCl_3$) [51]. As compared to TPAB, the aza-BODIPYs **13** and **16** with phenyl rings on the 1,7-positions exhibited 62 and 56 nm bathochromically shifted emission maxima in solution.

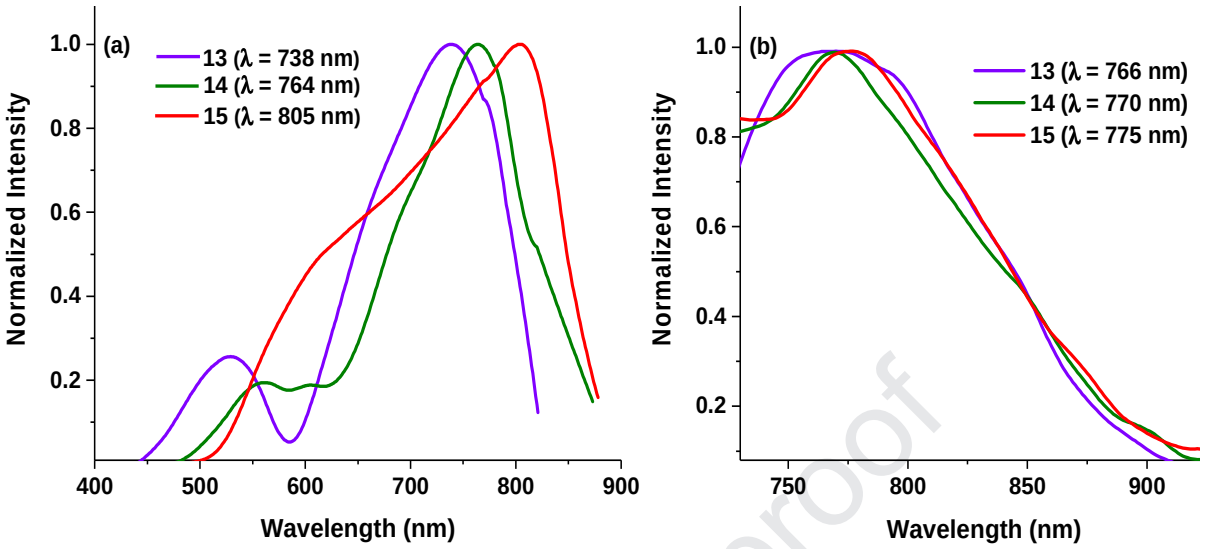

Figure 5. (a) Normalized absorption and (b) emission spectra of aza-BODIPYs **13** (λ_{ex} = 680 nm), **14** and **15** (λ_{ex} = 700 nm) on drop-cast film.

Whereas, the emission bands of aza-BODIPYs **14** and **15** having thiophene and *N*-butylcarbazole rings at 1,7-positions displayed red shifts of 81 and 98 nm, respectively as compared to TPAB. This could be attributed to the presence of electron donor substituents like thiophene and *N*-butylcarbazole on the aza-BODIPY core. However, the most red shifted emission maximum (790 nm) was observed for aza-BODIPY **15** in THF; making it a potential candidate for biological applications. The calculated emission quantum yields of aza-BODIPYs **13-15** were found to be in the range of 0.02 to 0.42 in toluene (Table 1); however owing to heavy atom effect lower quantum yield was observed for aza-BODIPY **16.** The solvent dependency of the absorption and emission of the compounds **13-16** was also studied (Table 1). However, only slight red shifts (2-8 nm) in the absorption and emission maxima were observed for **13**, **14** and **16**; this is a typical behavior observed for the BODIPY chromophores reported in literature. Nonetheless, the emission of aza-BODIPY **15** showed decent red shifts (10-20 nm) in polar solvents. Stokes shifts were found to be in the range of 520 to 1047 cm^{-1} for aza-BODIPYs **13-16.** The observed

bathochromic shifts in the emission bands of aza-BODIPYs, reveal larger dipoles of the CT excited states in polar solvents [52,53]. Particularly, the Stokes shifts of di-iodo aza-BODIPY **16** in polar solvents were much larger than the rest of the BODIPYs **13-15** (Table 1)**;** this can be explained by DFT studies. The HOMO-2 to LUMO transition in compound **16** is attributed to the ICT (intramolecular charge transfer) process (Figure 11); the electron density is spreaded on the donor TPE units in the HOMO-2 and the LUMO is clealry localized on the boron-dipyrrin core. Also, the larges dipole moment difference in the ground state and the excited CT state leads to electron phonon coupling with the solvent phonons; and the prescene of two iodine atoms on the 2,6-position of the BODIPY core results in the enhanced internal conversion and higher Stokes shifts in **16** [51,54]. The quantum yields of aza-BODIPYs **13-16** were slightly higher in non-polar solvent than those of in polar solvents (Table 1). In polar solvents the large dipole moment difference between ground state and charge-transfer excited state enable internal conversion in the molecules, resulting in the lower quantum yields [53].

To illustrate the potential of AIEE property arising from aza-BODIPYs **13-15** for solid state applications, the photophysical properties were examined on solid films. The thin films were prepared on glass plate by drop cast method and film based absorption and emission spectra of **13-15** are shown in figure 5. In solid state, aza-BODIPYs **13-15** exhibited significantly red shifted and comparatively broad absorption bands with 31, 40 and 67 nm shifts, , with respect to their corresponding absorption in solution state (Figure 5a). Typically, fluorophores display aggregation caused quenching (ACQ) of emission in solid state. In contrast, the aza-BODIPYs **13-15** exhibited moderately intense fluorescence in solid films at 766, 770 and 775 nm, respectively (Figure 5b). Furthermore, the solid state emission bands of **13-15** were broad and bathochromically shifted by 32, 17 and 5 nm, with respect to their corresponding emission in

solution phase. In general, BODIPYs with bulky substituents directly attached to the core reported to show solid state emission; since the steric crowding of large groups minimizes interchromophoric interactions in solid state. The amorphous films of aza-BODIPYs **13-15** prepared by drop-cast method, exhibited broad and red shifted absorption and emission due to the formation of parallel inclined π–π stacks of the molecules in solid state.

Heavy-Atom Effect and Singlet Oxygen Generation

In order to test the ability of aza-BODIPY **16** to produce singlet oxygen due to heavy atom effect; singlet oxygen generation study with 1,3-diphenylisobenzofuran (DPBF) was carried out [27]. The study was undertaken by monitoring the reaction of known singlet oxygen scavenger (DPBF) in solution with the singlet oxygen generated by our compound **16** (Figure 6). Due to the presence of two iodo groups on the aza-BODIPY core, compound **16** should have significant triplet population upon excitation at 633 nm, and can act as triplet sensitizer.

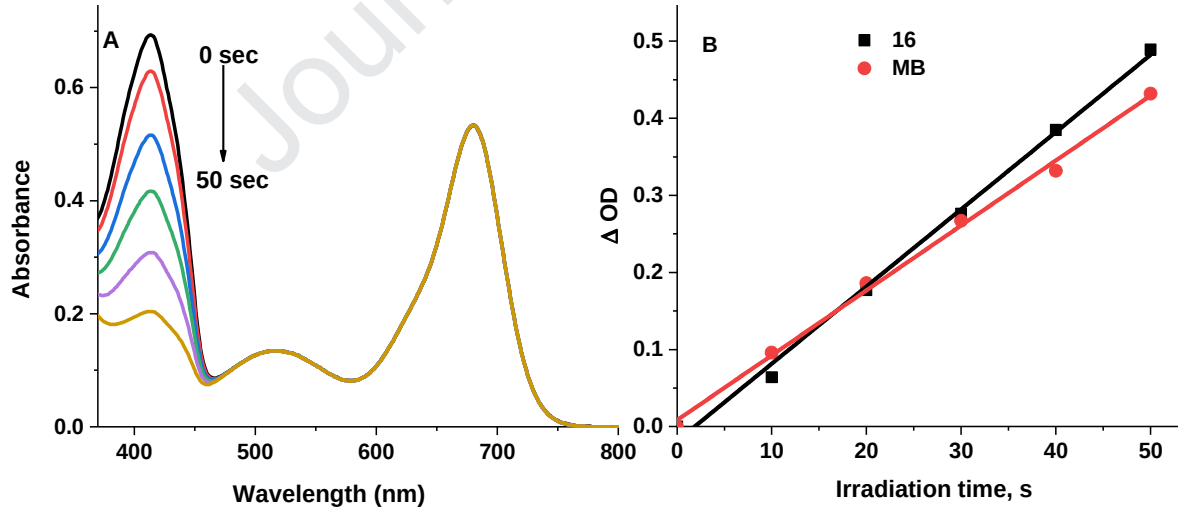

Figure 6. (a) Absorption spectra of DPBF (2 x 10^{-5} M) upon irradiation in the presence of aza-BODIPY **16** (1 x 10^{-5} M) from 0 to 50 sec (recorded at 10 sec interval) in DCM. Monochromatic light (633 nm at 0.5 mW/cm^2) was used; (b) Straight line plot of change in the absorbance of DPBF at 414 nm with the irradiation time in presence of aza-BODIPY **16** against methylene blue (**MB,** 3.1 x 10^{-6} M) as the standard in DCM.

The significant inter-system crossing (ISC) would lead to the energy transfer from photosensitizer (**16**) to triplet ground state of oxygen molecules; which in turn get excited to singlet state and react with DPBF. The disappearance of DPBF absorption band at 414 nm was monitored over a time period of 50 seconds. Monochromatic light source (633 nm at 0.5 mW/cm^2) was used to excite the aza-BODIPY **16**; as the time progressed the intensity of the DPBF absorption band at 414 nm gradually decreased (Figure 6a). The triplet photosensitization ability of compound **16** was compared with the reference photosensitizer (methylene blue, Φ_Δ = 0.57 in DCM) under similar conditions (Figure S5, SI) [27]. The singlet oxygen quantum yield, calculated for aza-BODIPY **16** was 0.68 in DCM; confirming that it has substantial spin-orbit coupling due to heavy atom effect. Moreover, the presence of iodo groups directly on the aza-BODIPY core in **16**, can considerably reduce the loss of excited state energy by non-radiative decay processes.

Energy Transfer Studies

Recent reports on BODIPYs based D-A systems demonstrated efficient FRET and TBET (through bond energy transfer) based molecular architectures. In the BODIPY based D-A systems, where TPE is used as donor the energy transfer process was named DRET (dark resonance energy transfer) [43]. DRET is similar to FRET phenomenon, though the donor chromophore is named “dark donor” as it is non-fluorescent in nature. According to the literature reports, the efficiency of energy transfer is reasonably high in DRET based system, because the loss of energy due to non-radiative decay is eliminated in the molecules [43]. Lately, TPE connected BODIPYs have been described with decent energy transfer from TPE donor to the BODIPY unit. TPE and its derivatives have been extensively studied for AIE properties, owing to facile synthetic modifications and high emission intensity in aggregated state. Atilgan and

coworkers [44] have reported D-A systems of BODIPY where, TPE is employed as “dark energy donor”. The intramolecular energy transfer in aza-BODIPYs **13-16** was evaluated by comparing the fluorescence emission of compounds excited at the donor and acceptor units in toluene (Table 2, Figure 7). The emission spectra of **13-16** in toluene displayed moderate emission intensity when excited at λ = 650 nm; the aza-BODIPY core absorbs strongly here. On the other hand, the fluorescence signals of **13-16** were very unusual when excited at λ = 330 nm; the TPE units absorb intensely here.

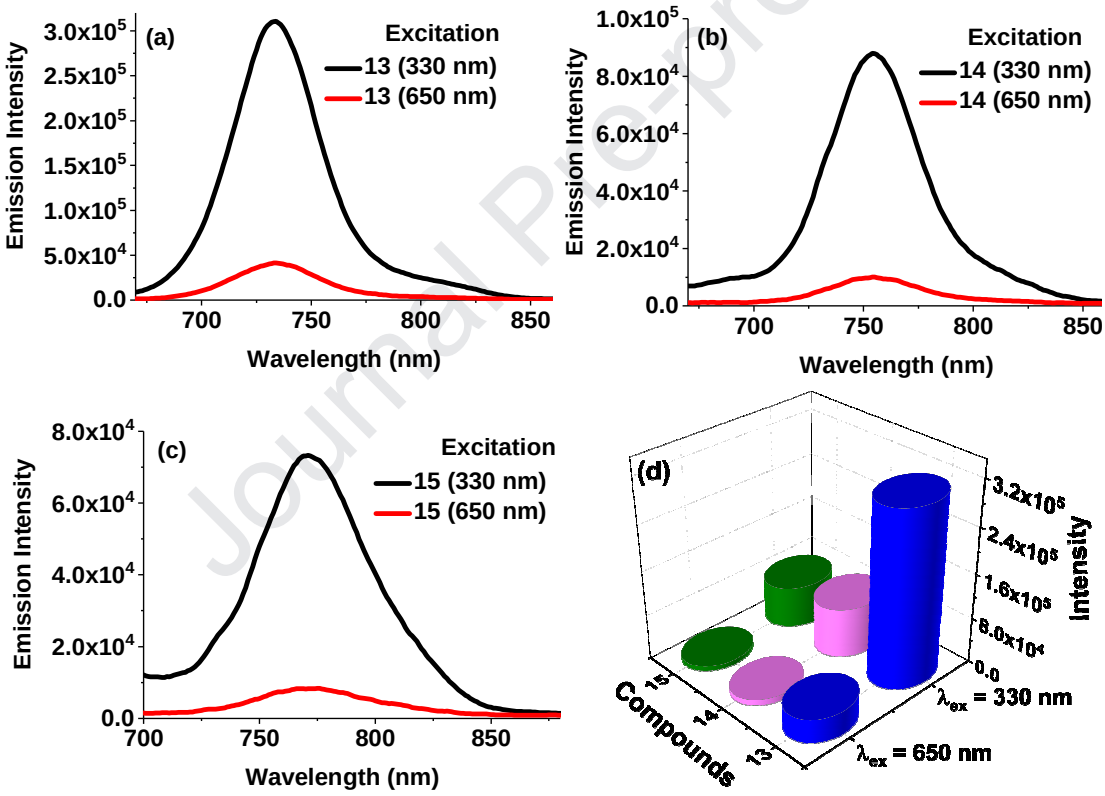

Figure 7. Comparative emission spectra of compounds: (A) **13,** (B) **14** and (C) **15** in toluene (2 x 10^{-6} M), excited at donor (black) and acceptor (red). (D) Comparative emission maxima of compounds **13**, **14** and **15** in toluene excited at donor and acceptor.

Table 2. Energy transfer data of aza-BODIPYs **13-16** in toluene.

Compound	Excitation (λ_{ex})	Emission (λ_{em})	Acceptor (Φ_f)	ETE (%)
TPAB[25]	650 nm	672 nm	–	–
13	650 nm	734 nm	0.42[b]	90%

	330 nm	734 nm	0.38[c]	
14	650 nm 330 nm	753 nm 754 nm	0.18[b] 0.14[c]	81%
15	650 nm 330 nm	771 nm 771 nm	0.08[b] 0.07[c]	88%
16	650 nm 330 nm	727 nm 731 nm	0.02[b] 0.014[c]	67%

b: Quantum yield of acceptor excited at acceptor; c: Quantum yield of acceptor excited at donor.

Intense fluorescence was observed from the aza-BODIPYs **13-16** in between 730 to 771 nm (Figure 7). This behavior can be explained by energy transfer phenomenon, where TPE units are donor and the aza-BODIPY unit is acting as acceptor. The compounds **13-16** were excited at two wavelengths, corresponding to the absorption of the donor (TPE units) and the acceptor (aza-BODIPY unit); then the fluorescence quantum yields were calculated (Table 2). The "energy transfer efficiency" (ETE, %) was calculated [52], which suggest the total energy transfer from donor to acceptor including non-radiative decays of the molecules in question [55]. The % ETE values are given in the table 2, suggesting effective intra-molecular energy transfer from TPE units to the aza-BODIPY unit in molecules **13-16**. Except diiodo aza-BODIPY (**16**), rest of the compounds exhibited ETE between 81-90%, which could be due to lack of fluorescence-leakage in these molecules. The pseudo-Stokes shifts [44] were calculated for compounds **13-16** by observing the difference between λ_{em} (aza-BODIPY core) and λ_{abs} (TPE); and the values were found to be in the range of 386 to 424 nm. The D-A systems **13-16** with high values of intramolecular energy transfer and huge pseudo-Stokes shifts are very attractive for prospective biological applications. The previous report on TPE substituted aza-BODIPY dimers [15] described the novel synthesis and AIE property of such molecules; though the energy transfer studies were not explored. To the best of our knowledge, molecules **13-16** are the first such TPE-aza-BODIPY conjugates which exhibit very large pseudo-Stokes shifts (386 to 424 nm). The

crystal structure of **13** showed that, the propeller shape TPE moieties and aza-dipyrrin core are not in the same plane; therefore possibility of energy transfer through space is not very favorable.

Femtosecond Transient Absorption Spectroscopy

In order to determine the exact time constants of the energy transfer process, we have performed femtosecond broadband transient absorption (TA) spectroscopy [27]. The molecule **13** consists of two different chromophores; one is the TPE and the other being the aza-BODIPY. The TPE chromophore absorbs around 350 nm and is non-fluorescent in nature. Whereas, the aza-BODIPY unit absorb around 650 nm; and emits at around 720 nm. The TA study was carried out in toluene and compound **13** was excited at 400 nm, to exclusively excite the molecules at the TPE chromophore.

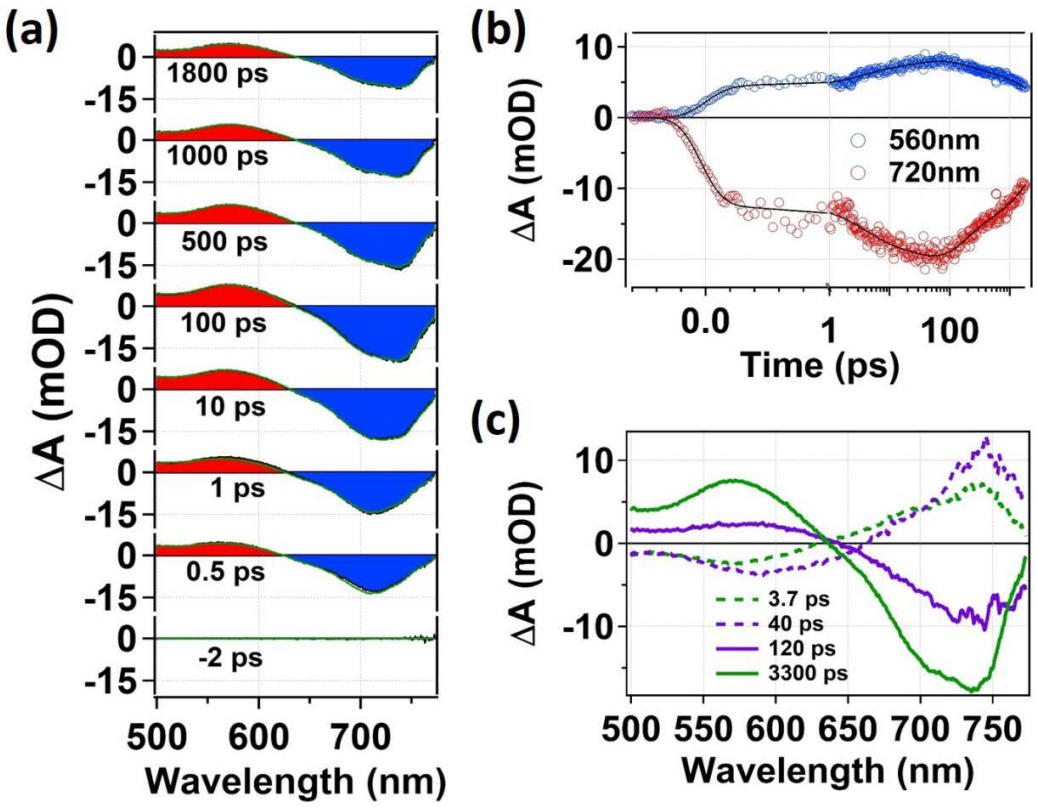

Figure 8. (a) TA spectra at some representative delay times along with the fitted spectra (green solid lines); (b) Kinetics at two representative wavelengths 560 nm and 720 nm along with the fitting (black solid lines); (c) Decay associated spectra (DAS) obtained from global analysis of the TA response of **13** in toluene after exciting at 400 nm.

The TA signal of **13** consists of a broad excited state absorption (ESA) band around 500-600 nm and a stimulated emission (SE) band centered at 720 nm (Figure 8a). The observation of the emission from aza-BODIPY unit in TA signal for **13** confirms the energy transfer process in the excited state. The TA responses of **13** were globally analyzed and successfully fitted with four different time constants; the fitted kinetics at two representative wavelengths is displayed in figure 8b. The observed time constants are 3.7 ps (τ_1), 40 ps (τ_2), 120 ps (τ_3) and 3300 ps (τ_4). Decay associated spectra (DAS, Figure 8c) for **13** show that the spectra associated with τ_1 is quite similar but of opposite sign compared to that of the spectra associated with τ_4. Which suggest that, τ_1 and τ_4 represent the formation and decay of a same state in the excited states manifold. Moreover, the spectra associated with τ_2 are same but negative of the DAS of τ_3. Thus τ_2 and τ_3 represent the formation and decay of another exited state species. It is clear from figure 8c that, though four different time constants are obtained from the global analysis, all DAS are quite similar. DAS spectra suggest that the two excited state species are structurally similar. The species associated with τ_1 and τ_4 is strongly emissive in nature, whereas the other one is weakly emissive. We suggest that, following is the singlet singlet energy transfer process; the excited state species undergo some kind of structural change to form the other species. A plausible pattern to describe the excited state phenomena of **13** is shown in scheme 4. We assign the 3.7 ps time constant as the time constant associated with energy transfer, which is also the formation time constant of the species [D-A*]. The lifetime of this species is 3300 ps. Following the energy transfer process [D-A*] structurally changes to [D-A*']. The formation time constant of this [D-A*'] is 40 ps and has a decay constant of 120 ps. The other molecules under investigation having

the similar donor-acceptor moieties are expected to exhibit similar dynamics. The experimental data for **15** is provided in the figure S52 of the supporting information.

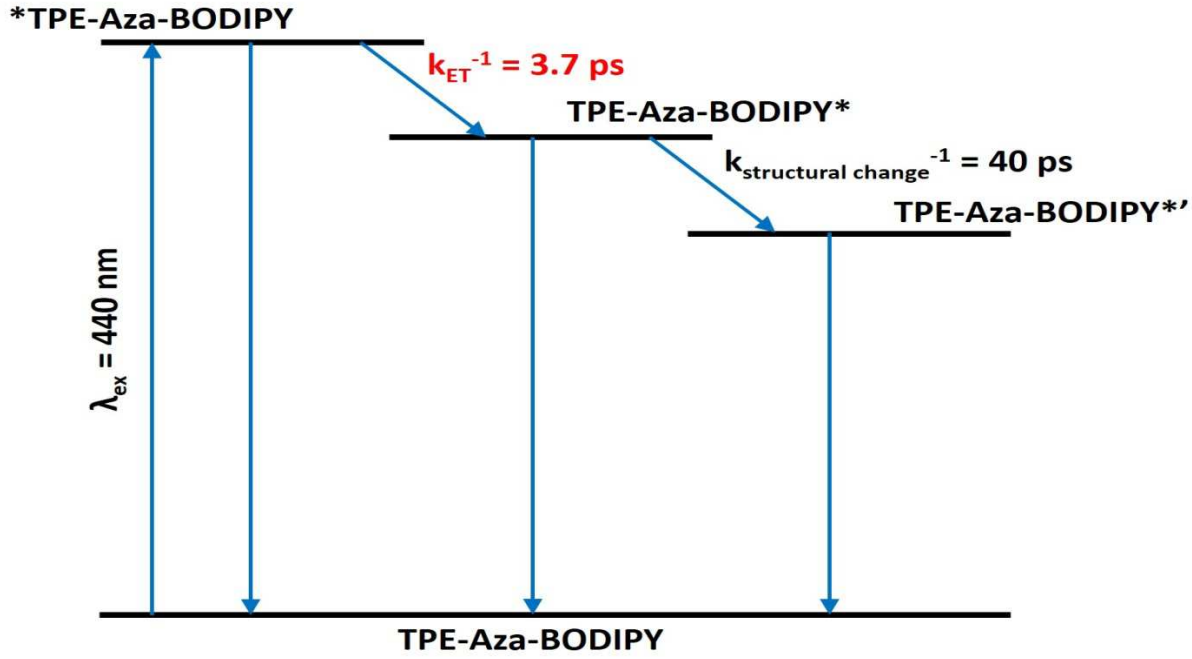

Scheme 4. Schematic of the excited state processes in aza-BODIPY **13**.

Aggregation Studies

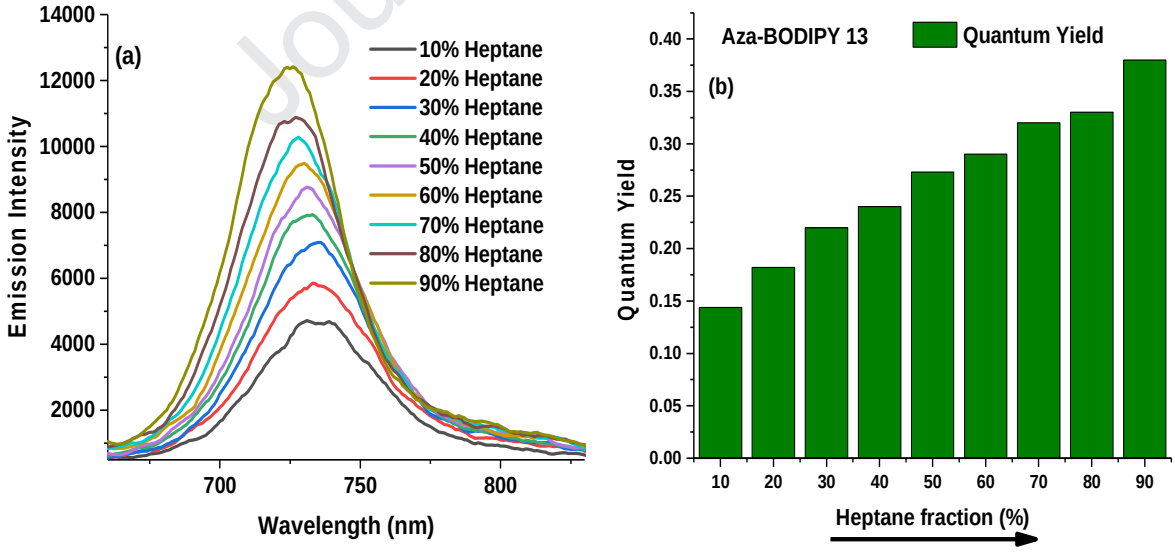

Figure 9. (a) Emission spectra of aza-BODIPY **13** in THF-heptane mixture with different heptane fractions. (b) Bar diagram of quantum yield of aza-BODIPY **13** with increasing heptane fractions.

Aggregation induced enhanced emission (AIEE) behavior of compounds **13-15** was investigated by promoting aggregate formation through alteration of solvent composition. The systematic change in the composition of THF/n-heptane solvent system from 100% THF to 90% n-heptane resulted in the formation of solid aggregates as indicated by the noticeable variations in the emission spectra. Compounds **13** and **14** showed AIEE phenomenon whereas, **15** exhibited aggregation caused quenching (ACQ) behavior. In pure THF, compounds **13** and **14** exhibited weak emissions at 735 nm (Φ_f = 0.14) and 754 nm (Φ_f = 0.10), respectively. However, upon increasing the volume fraction of n-heptane (f_h = 10% to 90%) in THF, the emission intensities were risen gradually (Figure 9). Moreover, the emission bands of **13** and **14** became narrower with significant blue shifts (~12 nm) in higher heptane fractions (f_h = 90%). At a f_h of 90%, significant (3-fold) increase in the emission intensity of aza-BODIPY **13** was observed and the calculated quantum yield was 0.44 (Table 3). The enhancement in the fluorescence intensity and quantum yields is due to AIEE behaviors of **13** and **14** (Table 3). The formation of AIEE active agglomerates of compounds **13** and **14** at f_h of 90% was confirmed by DLS. The size distribution pattern obtained from DLS showed that nano-aggregates formed are in range of 50-900 nm, having maximum probability distribution around 200-700 nm (Figure S6, SI). At f_h of 90%, the morphology of aggregates was further explored by SEM (Scanning Electron Microscopy) and the nano-aggregates were found to have spherical morphology. The size of nano-aggregates obtained from SEM analysis, was between 270-750 nm; which was in accordance with the DLS data (Figure S6, SI).

Electrochemical studies

The electrochemical properties of all aza-BODIPYs **13-15** were studied by cyclic voltammetry technique (Figure S3, SI). The cyclic voltammograms of aza-BODIPYs **13-15** were recorded in dry dichloromethane under N_2 atmosphere and the data is presented in table 3. The aza-BODIPYs **13-15** exhibited single irreversible oxidation wave in between 0.97 to 1.26 V. Aza-BODIPYs **13** and **14** showed two reversible reductions in between -0.32 to -1.13 V; whereas compound **15** showed three irreversible reduction waves in between -0.14 to -1.61 V. The oxidation potential of aza-BODIPY **13** was a bit anodically shifted as to those of the aza-BODIPY **14** and **15**; indicating that compound **13** was harder to oxidize.

Table 3. Electrochemical redox data (V vs SCE) of compounds **13-15** in DCM, recorded at 50 mV/s scan speed and energy levels calculated from optical CV data.

Compound	$E_{1/2}$(ox)/V	$E_{1/2}$(red)/V			HOMO	LUMO	ΔE [eV]	Optical ΔE
	I	I	II	III	[eV]	[eV]	(from CV)	[eV]
13	1.26	-0.38	-1.13	-	-5.68	-4.04	1.64	2.65
14	1.22	-0.32	-1.07	-	-5.64	-4.10	1.54	2.65
15	0.97	-0.14	-1.03	-1.61	-5.39	-4.28	1.11	2.63

The redox potential data was also used to determine the HOMO-LUMO energies (Table 3) of aza-BODIPYs **13-15**; the frontier orbital energies are presented in figure S4 (SI). In the aza-BODIPYs **13-15**, by varying the substituents at 1,7-positons from phenyl to thiophene and then to *N*-butylcarbazole the HOMO-LUMO gaps were decreased from 1.64 to 1.11 eV. Furthermore, the absorption data of compounds **13-15** was used to calculate the optical band gap (Table 3) [21]. As compared to compounds **14** and **15**, higher optical band gap was observed for the phenyl substituted compound (**13**). Among all the compounds, the lowest optical (2.63 eV) and electrochemical (1.11 eV) band gaps were obtained for compound **15**; which showed the most red shifted absorption and emission spectra as compared to the other aza-BODIPYs. The electron

rich *N*-butylcarbazole ring has considerable effect on the electronic property of the aza-BODIPY **15**.

Computational Studies

Ground state geometrical parameters

Density functional theory (DFT) and time dependent density functional theory (TD-DFT) were used to characterize the properties of ground and the low excited electronic states of the aza-BODIPY molecules **13-16.** The important structural parameters viz. bond lengths, valence angles and dihedral angles obtained as a result of geometry optimization are summarized in tables S4, S5 and S6 respectively (SI). Comparison of these structural parameters for the molecule **13** with the X-ray crystallographic structure is of immense importance. The X-ray crystallographic structure with C_2 symmetry cannot be visualized perfectly; therefore, average values of the structural parameters were used for the correlation. The numbering schemes for bond lengths, valance angles and for the dihedrals angles are provided in figures S7 and S8, respectively (SI). It is evident from tables S4 and S5 that the maximum deviation in bond lengths and valance angles for **13** with respect to the X-ray crystallographic structure is 0.02Å and 1.54° respectively. The maximum deviation in bond lengths is 0.005Å and the bond angles agree within the 0.46°; suggesting the sturdiness of the level of approximation used for the DFT study. Furthermore, the substituents at the aza-BODIPY skeleton have negligible effect on the optimized structures of compounds **13-16**.

Absorption studies

Theoretical simulations also provide the complementary spectroscopic understanding of the absorption properties of the molecules. To accomplish this, singlet-singlet electronic transitions

of the molecules **13-16** were calculated in $CHCl_3$ exclusively, owing to the insignificant effect of solvent polarities on the absorption profiles of these aza-BODIPYs. The type of transitions for the molecules **13-16** can be examined, prior to comparison of the lowest energy transitions (λ_{max}). For this purpose, topologies of the calculated molecular orbitals responsible for the transitions were figured out. The calculated frontier molecular orbitals (FMOs) and the absorption maxima along with their oscillatory strengths (*f*) are presented in figure S9 (SI) and table 4, respectively. It is apparent from the results that the most intense singlet-singlet transitions ($S_0 \rightarrow S_1$) of the molecule **13**, **14** and **16** are due to the electron promotion from HOMO→LUMO (89.78%, 92.48% and 54.08% for **13, 14** and **16** respectively) and HOMO-2→LUMO (8.0%, 5.78% and 42.32% for **13, 14** and **16** respectively), with the dominance of the former. Notably, for **13** the HOMO→LUMO transition is a $\pi \rightarrow \pi^*$ transition of the aza-BODIPY core; whereas, the HOMO-2→LUMO corresponds to a charge transfer from TPE chromophore to the aza–BODIPY unit. Similarly, for the molecule **14**, HOMO→LUMO and HOMO-2→LUMO transitions are the dominant $\pi \rightarrow \pi^*$ transitions occurring in the central core and the 1,7 substituted thiophene arms respectively. In contrast, HOMO→LUMO transition of the molecule **16** occurs via a charge transfer from TPE to the iodinated aza–BODIPY unit. On the other hand, HOMO-2→LUMO transition in **16,** is a mixture of intramolecular charge transfer from the TPE to the aza-BODIPY unit and $\pi \rightarrow \pi^*$ transition of the central core. In addition, the most intense singlet-singlet transition ($S_0 \rightarrow S_1$) of the molecule **15** is sheer HOMO→LUMO transition (98.0%).

Table 4: Calculated electronic excitation energies and corresponding oscillator strengths of the low-lying singlet excited state for the molecules **13-16** in $CHCl_3$.

Molecule	Theoretical					Experimental
	Electronic transition	Contribution	CI coefficients	Energy (nm)	Oscillatory strength (*f*)	Absorption in $CHCl_3$ (nm)
13	$S_0 \rightarrow S_1$	HOMO-2→LUMO HOMO→LUMO	0.20 0.67	671	1.12	703
14	$S_0 \rightarrow S_1$	HOMO-2→LUMO HOMO→LUMO	0.17 0.68	703	1.04	722
15	$S_0 \rightarrow S_1$	HOMO→LUMO	0.70	702	1.20	738
16	$S_0 \rightarrow S_1$	HOMO-2→LUMO HOMO→LUMO	0.46 0.52	584	0.85	680

*****CI coefficients are in absolute values.

This transition is an amalgam of $\pi \rightarrow \pi^*$ and charge transfer characteristics. The former occurs in the central core region whilst, the later takes place from the 1,7 substituted *N*-butylcarbazole arms to the central core of aza–BODIPY **15**. The substantial electronic communication between the substituents and the aza-BODIPY core is reflected with the delocalization of FMOs over the entire molecular framework. Analogous topologies of the LUMO of all the compounds (**13-16**) indicated strong electron accepting nature of the aza-BODIPY core. Despite the fact, that the numbers of absorption bands were seen in the calculated spectra of aza-BODIPYs **13-16**, but for the sake of brevity λ_{max} was chosen for the comparison. The calculated and observed λ_{max} values are accommodated in table 5. A significantly good agreement between the calculated and observed λ_{max} was seen for all the molecules except **16**. In particular, the maximum deviation of 96 nm was shown by **16**, followed by **15, 13** and **14** which have displayed the difference of 36 nm, 32 nm and 19 nm respectively. It is imperative to mention that, all the molecules were consistently underestimated, because of the limitations of vertical approximation.

In addition, the energies of FMOs and the HOMO-LUMO energy gap (ΔE) were calculated by employing DFT and TD-DFT approaches are summarized in table S7 (SI). The DFT calculation based energy level of HOMO and LUMO was found to be increased by 0.18 eV and 0.19 eV respectively, as we moved from aza-BODIPY **13-15**. In contrast, the experimental HOMO energy level was increased by 0.29 eV whereas; the LUMO energy level was decreased by 0.24 eV. Consequently, the calculated HOMO-LUMO energy gap was underestimated by 0.62 eV, 0.54 eV and 0.08 eV for the molecule **13**, **14** and **15** respectively. Similarly, the TD-DFT based HOMO-LUMO energy gap for aza-BODIPY **13, 14** and **15** were severely overestimated by 1.21 eV, 1.22 eV and 1.69 eV respectively from the electrochemical measurements. However, the TD-DFT based HOMO-LUMO energy gap was found to be in line with the optical measurements with an overestimation of 0.20 eV, 0.11 eV and 0.17 eV for **13**, **14** and **15** respectively. No such comparison was made for the molecule **16** owing to the unavailability of the experimental data.

Excited state geometrical parameters

In general, the electronic excitation of the molecules may result in the equilibrium geometries very different from those in their ground states. Therefore, the essential structural parameters viz. bond lengths, valence angles and dihedral angles of the S_1 of **13-16** were computed and compared with their corresponding S_0 geometrical parameters as presented in tables S4, S5 and S6 respectively (SI). It is evident from the tables S4 and S5 that, the valance angles and bond lengths of S_1 geometries are not significantly different from S_0 geometries for all the molecules. The utmost deviation in bond length and valance angle was found to be 0.027Å and 1.69° for **15** and **13** respectively. On the contrary, significant differences between S_0 and S_1 dihedral angles were notified for all the molecules under investigation as evident from table S6. To be more

precise, the maximum deviation in the dihedral angles were 9.11°, 14.62°, 5.77° and 7.32° for **13, 14, 15** and **16** respectively. Thus, from the above mentioned results one can conclude that the relaxation of the molecules **13-16** involve configurational change upon excitation.

Emission studies

It is a well-established fact that, the emission properties of a dye are more sensitive than its absorption [55]. Consequently, we have explored the emission spectra for **13-16** theoretically, to get the detailed insight about the nature of emission process. As per Kasha's rule, the fluorescence emission solely occurs from the S_1 state and prior to the possible emission to S_0, any electronic excitation to a higher state relaxes swiftly (10^{-14}-10^{-11} seconds) to S_1 [56]. The appropriate FMOs involved in the process of emission for **13** and **14-16** can be visualized from the figures 10, 11 and figure S10 (SI), respectively. The deactivation energies, transition composition and oscillatory strengths are accommodated in table 5. It is apparent from TD-DFT results that, the compounds **13-16** should have analogous excited state relaxation process as shown in figure 10, 11 for **13** and **16**, respectively.

Table 5: Computed electronic de-excitation energies and corresponding oscillator strengths of the low-lying singlet excited state for the molecules **13-16** in $CHCl_3$.

Molecule	Theoretical					Experimental
	Electronic transition	Contribution	CI coefficients	Energy (nm)	Oscillatory strength *(f)*	Emission in $CHCl_3$ (nm)
13	$S_0 \leftarrow S_1$	HOMO←LUMO	0.70	702	1.11	734
14	$S_0 \leftarrow S_1$	HOMO←LUMO	0.70	750	0.92	754
15	$S_0 \leftarrow S_1$	HOMO←LUMO	0.70	749	1.12	782
16	$S_0 \leftarrow S_1$	HOMO-2←LUMO HOMO←LUMO	0.22 0.67	635	0.91	729

*****CI coefficients are in absolute values.

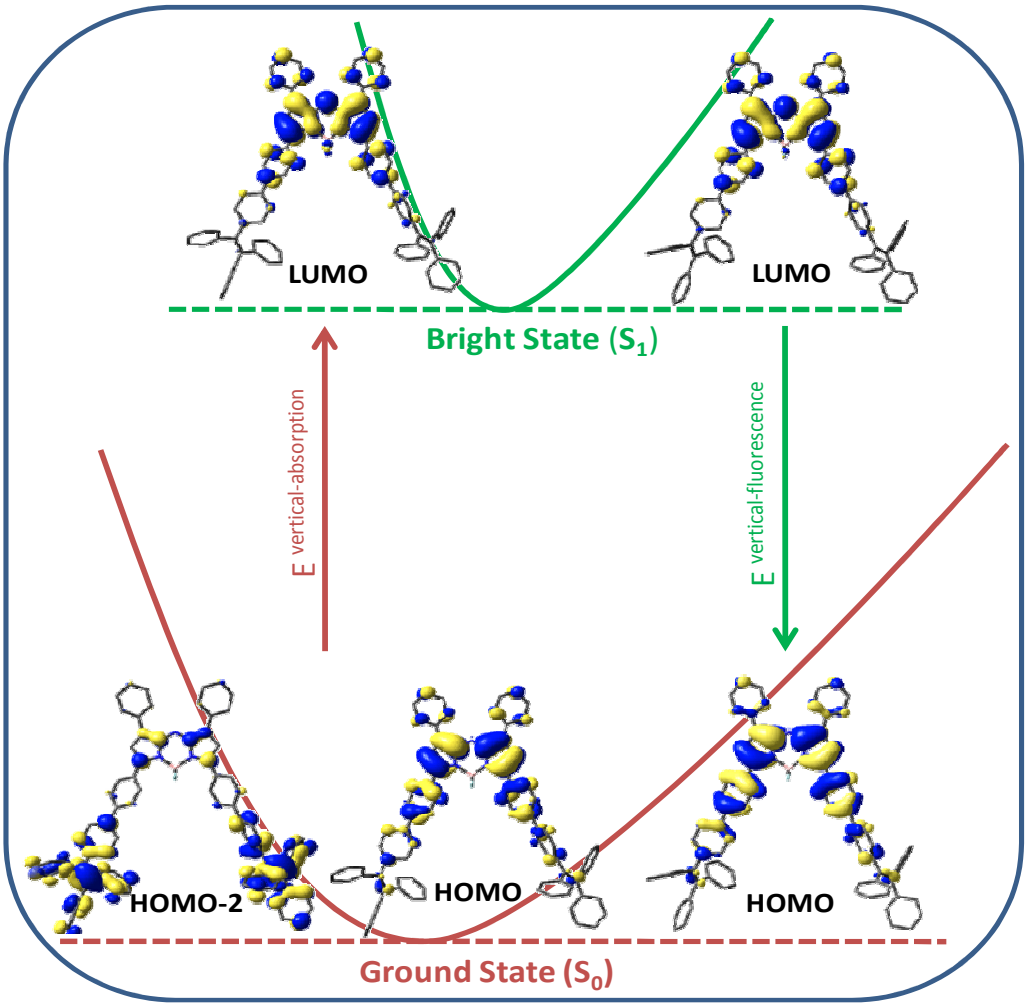

Figure 10: Scheme of the mechanism of fluorescence emission for the molecule **13.**

The major absorption of the molecules **13-16** mainly comprises of π→π* transitions; and upon excitation the electron gets promoted to S_1, which finally relaxes to S_0 (Figure S10 for **14** and **15**, SI). The oscillatory strengths for $S_1 \rightarrow S_0$ transitions for **13, 14, 15** and **16** are 1.11, 0.92, 1.12 and 0.91, respectively. The S_1 state of all the compounds (**13-16**) are bright states, which make the relaxation transitions allowed and therefore decays via radiative manner (fluorescence). This is clearly reflected from the red shift in the emission wavelengths in comparison to their absorption wavelengths as shown in table S8.

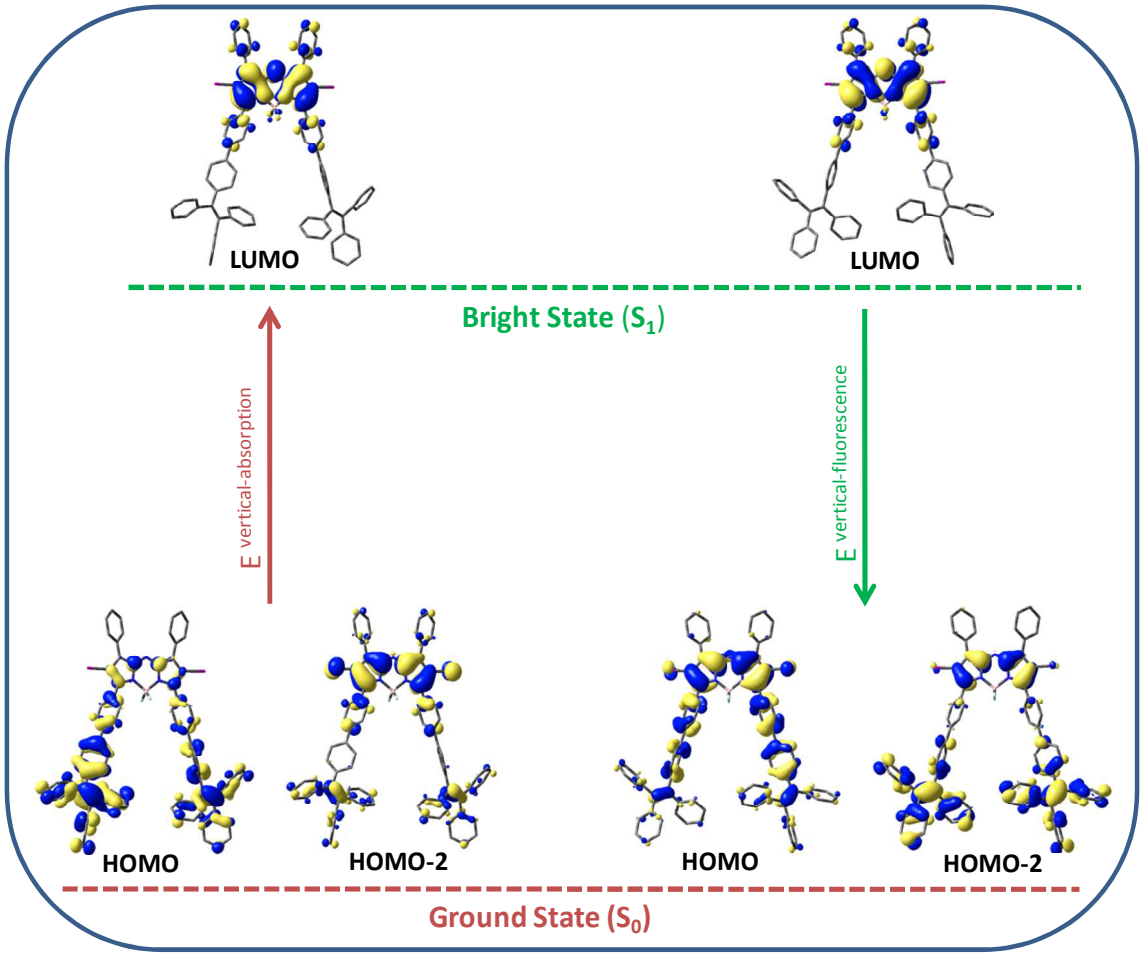

Figure 11: Scheme of the mechanism of fluorescence emission for the molecule **16.**

In addition, the TD-DFT calculations based fluorescence energies were underestimated compared to the experimental emission energies. The utmost deviation of 94 nm was displayed by **16**, followed by **15, 13** and **14** which have shown the difference of 33 nm, 32 nm and 4 nm respectively. However, the significantly good agreement between the experimental and calculated Stokes shifts was observed for all the molecules as shown in table S8.

Conclusion

In summary, we have synthesized and studied the absorption, transient absorption, emission, aggregation and electrochemical properties of the TPE connected aza-BODIPYs. In addition, the

complementary spectroscopic insight into the roots of absorption and emission profiles was furnished via TD-DFT studies. The substituents on the 1,7-positions of aza-BODIPYs were varied from phenyl, thiophene to *N*-butylcarbazole. Also, TPE units were linked at the *para* positions of 3,5-phenyls of the aza-BODIPYs. The significant red shifts (35-88 nm) in absorption and (56-98 nm) in the emission spectra, were observed for the TPE linked aza-BODIPYs as compared to parent TPAB; this could be attributed to extended electronic communications between the 1,7- substituents and the aza-BODPY core. Among all aza-BODIPYs, the most red shifted absorption and emission were observed for aza-BODIPY having *N*-butylcarbazole and TPE groups on the core; this compound also exhibited lowest HOMO-LUMO energy gap calculated by electrochemical method. Aggregation studies in THF/n-heptane solution showed hypsochromic shifts in the aggregated form; X-ray packing structures indicated H-type aggregates (slip angle > 54.7^{o}) in the solid state. All donor-acceptor type aza-BODIPYs exhibited efficient intramolecular energy transfer from TPE donor to the fluorescent aza-BODIPY acceptor. The energy transfer efficiencies were found to be 81-90% in all the D-A aza-BODIPYs; and very large (386 to 424 nm) pseudo Stokes shifts were observed in solution. Transient absorption studies also supported energy transfer phenomenon and the time constant associated with ET was 3.7 ps. An introduction of AIE active chromophore (energy donor) on the aza-BODIPY skeleton can be another strategy to make ET based NIR dyes with large pseudo Stokes shifts.

Acknowledgements

Financial support from and SERB, Govt. of India (Grant No: **EMR/2015/000779**) is duly acknowledged. IG is grateful to Prof. H. Furuta, Kyushu University, Japan for X-ray

measurements. NB, NM and MYL thank IIT Gandhinagar for fellowship and infrastructural support.

Supporting Information

The mass and heteronuclear NMR characterization data, X-ray structure parameters and DFT calculations details and optimized geometries of the reported compounds are available.

Experimental

Instrumentation and Reagents

All the reagents and solvents were purchased from Aldrich and used without further purification; silica gel (60-120 mesh size) for column chromatography was acquired from Merck. The di-isopropylamine (DIEA) and dichloromethane (DCM) and were dried prior to use for studies and synthesis. The NMR data were recorded with Bruker Avance III 500 MHz NMR spectrometer. The ESI-MS data were obtained from Waters Synapt-G2S ESI-Q-TOF Mass instrument. The MALDI-MS data for some of the compounds were acquired with Bruker Daltonics UltrafleXtreme MALDI-TOF instrument. Shimadzu UV-1700 spectrometer was used to record the absorption spectra. Solid state absorption spectra were recorded with Agilent Technologies Cary series UV-Vis NIR spectrometer (MY1740000600). Fluorescence emission (solution as well as solid state) measurements were recorded with Horiba-Jobin Yvon Fluorlog-3 spectrometer.

Computational methodology

All the computations performed in the present contribution were accomplished by using Gaussian 09 program [57]. The ground-state (S_0) geometry optimization of the molecules **13-16** were carried out without symmetry constraints by using parameter free Perdew, Burke and

Ernzerhof hybrid functional PBE1PBE [58,59]; along with the split-valence atomic basis set 6-311G(2d,p) for all the atoms except iodine for which LANL2DZ was used [60].

General Procedure for Chalcones (1-3) The mixture of aromatic aldehyde (1 equiv.) and 4-bromoacetophenone (1 equiv.) was dissolved in methanol/water (1:1 mixture). After five minutes NaOH (0.1 equiv.) was added and reaction mixture was refluxed for 2 h. The product was precipitated as yellow solid. Reaction mixture was extracted with DCM and dried over anhydrous Na_2SO_4 and solvent was evaporated by using rotary evaporator under reduced pressure. The crude product was subjected to silica gel column chromatography for purification.

Compound (1) Benzaldehyde (2.0 g, 1.9 mL, 18.84 mmol), 4-bromoacetophenone (3.8 g, 18.84 mmol) and NaOH (75 mg, 1.88 mmol) were reacted in methanol/water (21 mL) mixture as per the general procedure. The desired product **1** was purified by silica gel column using 20% DCM/hexane as solvent mixture. Brown solid, Yield: 57% (3.10 g). R_f = 0.23 (silica, DCM/hexane 1:4). ^{1}H NMR ($CDCl_3$, 500 MHz, δ ppm): 7.88 (d, J = 8 Hz, 2H), 7.82 (d, J = 15.5 Hz, 1H), 7.65 (d, J = 7.5 Hz, 4H), 7.45 (m, 4H). ^{13}C NMR ($CDCl_3$, 125 MHz, δ ppm): 189.38, 145.40, 136.98, 134.74, 131.95, 130.75, 130.04, 129.02, 128.52, 127.89, 121.56. HRMS (ESI-Q-TOF): $C_{15}H_{12}BrO^+$ $[M+H]^+$ calcd: m/z 287.0072; found: m/z 287.0081.

Compound (2) 2-Thiophenecarbaldehyde (2.0 g, 1.7 mL, 17.83 mmol), 4-bromoacetophenone (3.5 g, 17.83 mmol) and NaOH (71 mg, 1.78 mmol) were reacted in methanol/water (21 mL) mixture as per the general procedure. The desired product **2** was purified by silica gel column using 25% DCM/hexane as solvent mixture. Yellow solid, Yield: 66% (3.45 g). R_f = 0.22 (silica, DCM/hexane 1:4). ^{1}H NMR ($CDCl_3$, 500 MHz, δ ppm): 7.94 (d, J = 15.5 Hz, 1H), 7.87 (d, J = 8 Hz, 2H), 7.64 (d, J = 8 Hz, 2H), 7.44 (d, J = 5 Hz, 1H), 7.37 (d, J = 3 Hz, 1H), 7.27 (d, J = 14.5

Hz, 1H), 7.10 (t, *J* = 4.5 Hz, 1H). ^{13}C NMR ($CDCl_3$, 125 MHz, δ ppm): 188.71, 140.24, 137.73, 136.90, 132.35, 131.94, 129.93, 129.10, 128.44, 127.87, 120.19. HRMS (ESI-Q-TOF): $C_{13}H_{10}BrOS^+$ $[M+H]^+$ calcd: *m*/*z* 292.9636, found; *m*/*z* 296.9615.

Compound (3) *N*-butylcarbzolealdehyde (2.0 g, 7.95 mmol), 4-bromoacetophenone (1.6 g, 7.95 mmol) and NaOH (32 mg, 0.79 mmol) were reacted in methanol/water (21 mL) mixture as per the general procedure. The desired product **3** was purified by silica gel column using 25% DCM/hexane as solvent mixture. Yellow solid, Yield: 64% (2.20 g). R_f = 0.20 (silica, DCM/hexane 1:3). ^{1}H NMR ($CDCl_3$, 500 MHz, δ ppm): 8.37 (s, 1H), 8.13 (d, *J* = 8 Hz, 1H), 8.05 (d, *J* = 15.5 Hz, 1H), 7.93 (d, *J* = 8.5 Hz, 2H), 7.77 (d, *J* = 8.5 Hz, 1H), 7.65 (d, *J* = 8.5 Hz, 2H), 7.52 (d, *J* = 15 Hz, 2H), 7.43-7.40 (m, 2H), 7.29 (t, *J* = 7.5 Hz, 1H), 4.31 (t, *J* = 7.5 Hz, 2H), 1.90-1.84 (m, 2H), 1.44-1.37 (m, 2H), 0.95 (d, *J* = 7.5 Hz, 3H). ^{13}C NMR ($CDCl_3$, 125 MHz, δ ppm): 189.37, 147.11, 142.13, 141.02, 137.57, 131.82, 130.00, 127.41, 126.40, 126.39, 125.72, 123.44, 122.77, 121.74, 120.60, 119.79, 118.39, 109.22, 109.19, 43.07, 31.11, 20.54, 13.87. HRMS (ESI-Q-TOF): $C_{25}H_{23}BrNO^+$ $[M+H]^+$ calcd: *m*/*z* 432.0963, found; *m*/*z* 432.0954.

General Procedure for compounds (4-6) A chalcone (1 equiv.) was dissolved in ethanol, then nitromethane (20 equiv.) and KOH (0.2 equiv.) were added in the reaction flask. The reaction mixture was refluxed for 12 h; as the reaction progressed, the color changed from light yellow to black. Reaction mixture was extracted with ethyl acetate and dried over anhydrous Na_2SO_4 and solvent was evaporated by using rotary evaporator. The desired product was subjected to silica gel column chromatography for purification.

Compound (4) Chalcone **1** (2.5 g, 8.70 mmol), nitromethane (9.3 mL, 174.12 mmol) and KOH (98 mg, 1.74 mmol) were refluxed in ethanol (80 mL) as per general procedure. The desired product **4** was purified by silica gel column using 6% ethyl acetate/hexane mixture. Brown oil,

Yield: 70% (2.12 g). R_f = 0.20 (silica, DCM/hexane 1:1). ^{1}H NMR ($CDCl_3$, 500 MHz, δ ppm): 7.76 (d, *J* = 9 Hz, 2H), 7.58 (d, *J* = 8.5 Hz, 2H), 7.34-7.31 (m, 2H), 7.28-7.26 (m, 3H), 4.82-4.78 (m, 1H), 4.70-4.65 (m, 1H), 4.22-4.17 (m, 1H), 3.45-3.36 (m, 2H). ^{13}C NMR ($CDCl_3$, 125 MHz, δ ppm): 195.89, 138.94, 135.12, 132.09, 129.54, 129.14, 128.84, 127.99, 127.44, 79.51, 41.49, 39.27. MS (ESI-Q-TOF): $C_{16}H_{14}BrO^+$ $[M\text{-}NO_2]^+$ calcd: *m*/*z* 301.0228, found; *m*/*z* 301.0326.

Compound (5) Chalcone **2** (3.5 g, 11.76 mmol), nitromethane (12.6 mL, 235.35 mmol) and KOH (132 mg, 2.35 mmol) were reacted in ethanol (80 mL) as per general procedure. The desired product **5** was purified by silica gel column using 6% ethyl acetate/hexane mixture. Brown oil, Yield: 49% (2.04 g). R_f = 0.20 (silica, DCM/hexane 1:1); ^{1}H NMR ($CDCl_3$, 500 MHz, δ ppm): 7.79 (d, *J* = 8.5 Hz, 2H), 7.61 (d, *J* = 8.5 Hz, 2H), 7.21 (d, *J* = 5 Hz, 1H), 6.95-6.93 (m, 2H), 4.84-4.81 (m, 1H), 4.73-4.69 (m, 1H), 4.56-4.50 (m, 1H), 3.52-3.42 (m, 2H). ^{13}C NMR ($CDCl_3$, 125 MHz, δ ppm): 195.50, 141.64, 135.00, 132.14, 129.56, 128.99, 127.21, 125.65, 124.82, 79.77, 42.26, 34.74. MS (ESI-Q-TOF): $C_{14}H_{12}BrOS^+$ $[M\text{-}NO_2]^+$ calcd: *m*/*z* 306.9792, found; *m*/*z* 306.9904.

Compound (6) Chalcone **3** (2.0 g, 4.62 mmol), nitromethane (4.9 mL, 92.52 mmol) and KOH (51 mg, 0.92 mmol) were reacted in ethanol (70 mL) as per the general procedure. The desired product **6** was purified by silica gel column using 6% ethyl acetate/hexane mixture. Brown oil, Yield: 57% (1.32 g). R_f = 0.28 (silica, DCM/hexane 1:1). ^{1}H NMR ($CDCl_3$, 500 MHz, δ ppm): 8.05 (d, *J* = 7.5 Hz, 1H), 7.96 (s, 1H), 7.77 (d, *J* = 8.5 Hz, 2H), 7.57 (d, *J* = 8.5 Hz, 2H), 7.47-7.44 (m, 1H), 7.38 (d, *J* = 8.5 Hz, 1H), 7.34 (d, *J* = 1 Hz, 2H) 7.23-7.20 (m, 1H). ^{13}C NMR ($CDCl_3$, 125 MHz, δ ppm): 196.22, 140.86, 139.97, 135.28, 132.03, 129.57, 129.10, 128.69, 126.01, 124.89, 123.25, 122.36, 120.41, 119.12, 118.98, 109.23, 108.85, 42.94, 42.24, 39.57,

31.14, 20.56, 13.87. MS (ESI-Q-TOF): $C_{26}H_{26}BrN_2O_3^+$ $[M+H]^+$ calcd: *m/z* 493.1127, found; *m/z* 493.1346.

General Procedure for Aza-Dipyrrins (7-9) Compound (**4** or **5** or **6**, 1 equiv.) was dissolved in 15.00 mL ethanol and NH_4OAc (35 equiv.) was added to it. The reaction mixture was allowed to stir for 48 h towards; after 12h product was precipitated as blue solid. The crude product was filtered and washed with cold ethanol to obtain pure aza-dipyrrins.

Compound (7) Compound **4** (2.1 g, 5.74 mmol) was reacted with NH_4OAc (15.5 g, 201.03 mmol) in ethanol (40 mL) as per the general procedure to get aza-dipyrrin **7**. Blue solid, Yield: 22% (0.82 g). R_f = 0.24 (silica, DCM/hexane 1:2). ^{1}H NMR ($CDCl_3$, 500 MHz, δ ppm): 8.03 (d, *J* = 7.5 Hz, 4H), 7.77 (d, *J* = 8 Hz, 4H), 7.66 (d, *J* = 7.5 Hz, 4H), 7.43-7.41 (m, 4H), 7.38-7.35 (m, 2H), 7.15 (s, 2H). MS (MALDI-TOF): $C_{32}H_{21}Br_2N_3^+$ $[M]^+$ calcd: *m/z* 607.0082; found: *m/z* 607.034

Compound (8) Compound **5** (2.0 g, 5.64 mmol) was reacted with NH_4OAc (15.2 g, 197.61 mmol) in ethanol (40 mL) as per the general procedure to get aza-dipyrrin **8**. Blue solid, Yield: 20% (0.74 g). R_f = 0.22 (silica, DCM/hexane 1:2). ^{1}H NMR ($CDCl_3$, 500 MHz, δ ppm): 7.83 (d, *J* = 3 Hz, 2H), 7.71 (d, *J* = 8 Hz, 4H), 7.63 (d, *J* = 8 Hz, 4H), 7.43 (d, *J* = 5 Hz, 2H), 7.14 (t, *J* = 4 Hz, 2H), 7.01 (s, 2H). MS (MALDI-TOF): $C_{28}H_{17}Br_2N_3S_2^+$ $[M]^+$ calcd: *m/z* 618.9210; found: *m/z* 618.034.

Compound (9) Compound **6** (2.0 g, 4.05 mmol) was reacted with NH_4OAc (10.9 g, 141.87 mmol) in ethanol (40 mL) as per the general procedure. Blue solid **9**, Yield: 16% (0.61 g). R_f = 0.20 (silica, DCM/hexane 1:1.5). ^{1}H NMR ($CDCl_3$, 500 MHz, δ ppm): 8.76 (s, 2H), 8.28 (d, *J* = 8.5 Hz, 2H), 7.86 (d, *J* = 7.5 Hz, 2H), 7.77 (d, *J* = 8 Hz, 4H), 7.61 (d, *J* = 7 Hz, 4H), 7.42-7.36 (m, 4H), 7.28 (s, 2H), 7.17 (s, 2H), 7.02 (t, *J* = 7.5 Hz, 2H), 4.18 (d, *J* = 7.5 Hz, 4H), 1.82-1.76

(m, 4H), 1.39-1.31 (m, 4H), 0.91 (t, *J* = 7.5 Hz, 6H). MS (MALDI-TOF): $C_{52}H_{43}Br_2N_5^+$ $[M]^+$ calcd: *m/z* 897.1865; found: *m/z* 897.330.

General Procedure for TPE Aza-Dipyrrins (10-12) The aza-dipyrrins (**7** or **8** or **9**, 1 equiv.) and tetraphenylethylene boronic acid (TPE boronic acid) (2.2 equiv.) were dissolved in dry toluene. After 5 minutes $Pd(PPh_3)_4$ (0.046 equiv.) was added in the reaction flask. Then ethanol and 2M K_2CO_3 were added and reaction mixture was refluxed for 24 h at 85 ^oC. The reaction mixture was extracted with ethyl acetate and dried over anhydrous Na_2SO_4 and solvent was dried. The crude reaction product was washed with cold ethanol and the solid blue product was directly used for the next step without column chromatography.

Compound (10) The aza-dipyrrin **7** (200.0 mg, 0.33 mmol), TPE boronic acid (273.2 mg, 0.72 mmol), $Pd(PPh_3)_4$ (17.5 mg, 0.015 mmol) were mixed in dry toluene (5 mL). Then ethanol (2 mL) and 2M K_2CO_3 (2 mL) were added and general method followed to get compound **10**, black maroon solid. Crude yield: 25% (94 mg). MS (MALDI-TOF): $C_{84}H_{60}N_3$ $[M+H]^+$ calcd: *m/z* 1110.7487; found: *m/z* 1110.651.

Compound (11) The aza-dipyrrin **8** (150.0 mg, 0.24 mmol), TPE boronicacid (200.5 mg, 0.53 mmol) and $Pd(PPh_3)_4$ (12.8 mg, 0.011 mmol) were mixed in dry toluene (5 mL). Then ethanol (2 mL) and 2M K_2CO_3 (2 mL) were added general method followed to get compound **11**, as blue solid. Crude yield: 25% (68 mg). MS (MALDI-TOF): $C_{80}H_{56}N_3S_2$ $[M+H]^+$ calcd: *m/z* 1122.3916; found: *m/z* 1122.554.

Compound (12) The aza-dipyrrin **9** (300.0 mg, 0.33 mmol), TPE boronic acid (276.5 mg, 0.73 mmol) and $Pd(PPh_3)_4$ (17.7 mg, 0.015 mmol) were mixed in dry toluene (5 mL). Then ethanol (2 mL) and 2M K_2CO_3 (2 mL) were added and general method followed to get compound **12,** as

bluish green solid. Crude yield: 17% (82 mg). MS (MALDI-TOF): $C_{104}H_{81}N_5$ $[M]^+$ calcd: *m/z* 1400.6526; found: *m/z* 1400.891

General Procedure for Aza-BODIPYs (13-15)

In a clean dry two necked 250 mL round-bottomed flask, aza-dipyrrin (**10** or **11** or **12**, 1 equiv.) was taken under inert atmosphere. Dry dichloromethane (DCM, 11 equiv.) and dry diisopropylethylamine (DIPEA, 11 equiv.) were added in the flask. After 15 min. $BF_3.OEt_2$ (15.6 equiv.) was added and reaction mixture was stirred for 24 hours at room temperature. The color of the reaction mixture changed from blue to green, then it was quenched with water and extracted with dichloromethane. Solvent was dried over anhydrous Na_2SO_4 and evaporated on rotary evaporator; crude aza-BODIPYs (**13-15**) were subjected to silica gel column chromatography. The desired products were purified by column chromatography on silica gel and eluted with 40% DCM/hexane.

Compound (13) The aza-dipyrrin **10** (80.0 mg, 0.072 mmol) and $BF_3.OEt_2$ (0.13 mL, 1.12 mmol) were reacted in DCM (0.05 mL) /DIPEA (0.13 mL) mixture as per the general procedure to get pure aza-BODIPY **13** as metallic green solid. Yield: 38% (32 mg). R_f = 0.18 (silica, DCM/hexane 1:2). ^{1}H NMR ($CDCl_3$, 500 MHz, δ ppm): 8.13 (d, *J* = 8 Hz, 4H), 8.07 (d, *J* = 7 Hz, 4H), 7.68 (d, *J* = 8 Hz, 4H), 7.46-7.41 (m, 8H), 7.12-7.05 (m, 38H). ^{13}C NMR ($CDCl_3$, 125 MHz, δ ppm): 158.66, 145.84, 143.83, 143.70, 143.69, 143.66, 143.62, 142.99, 141.50, 140.46, 137.72, 132.39, 131.93, 131.44, 131.36, 130.27, 130.20, 129.45, 129.39, 128.63, 127.83, 127.76, 127.67, 126.95, 126.63, 126.57, 126.51, 126.29, 119.12. ^{19}F NMR (470.4 MHz, $CDCl_3$, δ ppm): -131.40 (q, 2F). ^{11}B NMR (160 MHz, $CDCl_3$, δ ppm): 1.07 (t, 1B). MS (ESI-Q-TOF): $C_{84}H_{59}BF_2N_3^+$ $[M+H]^+$ calcd: *m/z* 1158.4770; found: *m/z* 1158.4749.

Compound (14) The aza-dipyrrin **11** (70.0 mg, 0.06 mmol) and $BF_3.OEt_2$ (0.12 mL, 0.97 mmol) were reacted in DCM (0.05 mL) / DIEA (0.12 mL) mixture as per the general procedure to afford pure aza-BODIPY **14** as metallic green solid. Yield: 48% (35 mg). R_f = 0.18 (silica, DCM/hexane 1:2). ^{1}H NMR ($CDCl_3$, 500 MHz, δ ppm): 8.12 (d, *J* = 8.5 Hz, 4H), 7.96 (d, *J* = 3 Hz, 2H), 7.69 (d, *J* = 8 Hz, 4H), 7.58 (d, *J* = 4.5 Hz, 2H), 7.45 (d, *J* = 8.5 Hz, 4H), 7.22 (t, *J* = 4.5 Hz, 2H), 7.16-7.08 (m, 34H), 6.99 (s, 2H). ^{13}C NMR ($CDCl_3$, 125 MHz, δ ppm): 158.59, 145.20, 143.73, 143.68, 143.65, 142.88, 141.50, 141.50, 140.49, 137.97, 137.75, 134.80, 132.73, 131.94, 131.46, 131.38, 130.24, 130.14, 129.66, 128.28, 127.85, 127.78, 127.73, 127.69, 127.63, 126.88, 126.66, 126.59, 126.52, 126.40, 126.29, 116.76, 114.63. ^{19}F NMR (470.4 MHz, $CDCl_3$, δ ppm): -130.36 (q, 2F). ^{11}B NMR (160 MHz, $CDCl_3$, δ ppm): 0.98 (t, 1B). MS (ESI-Q-TOF): $C_{80}H_{55}BF_2N_3S_2^+$ $[M+H]^+$ calcd: *m*/*z* 1170.3899; found: *m*/*z* 1170.5956.

Compound (15) The aza-dipyrrin **12** (80.0 mg, 0.05 mmol) and $BF_3.OEt_2$ (0.11 mL, 0.89 mmol) were reacted in dry DCM (0.04 mL) /dry DIEA (0.10 mL) mixture as per the general procedure to afford **15** as metallic green solid. Yield: 46% (38 mg). R_f = 0.16 (silica, DCM/hexane 1:2). ^{1}H NMR ($CDCl_3$, 500 MHz, δ ppm): 8.93 (s, 2H), 8.37 (d, *J* = 8.5 Hz, 2H), 8.17 (d, *J* = 8.5 Hz, 4H), 8.00 (d, *J* = 7.5 Hz, 2H), 7.69 (d, *J* = 8.5 Hz, 4H), 7.44-7.41 (m, 10H), 7.14-7.05 (m, 38H), 4.27 (t, *J* = 7.5 Hz, 4H), 1.87-1.81 (m, 4H), 1.42-1.35 (m, 4H), 0.93 (t, *J* = 7.5 Hz, 6H). ^{13}C NMR ($CDCl_3$, 125 MHz, δ ppm): 157.83,154.05, 143.91, 143.68, 140.54, 140.46, 139.29, 137.98, 136.40, 132.73, 131.89, 131.45, 131.37, 131.34, 131.32, 130.07, 127.82, 127.74, 127.71, 127.66, 127.61, 126.85, 126.38, 126.28, 122.14, 119.26, 114.60, 109.20, 108.98, 43.06, 33.83, 31.94, 29.70, 22.70, 20.53, 13.84 . ^{19}F NMR (470.4 MHz, $CDCl_3$, δ ppm): -130.48 (q, 2F). ^{11}B NMR (160 MHz, $CDCl_3$, δ ppm): 1.16 (t, 1B). MS (ESI-Q-TOF): $C_{104}H_{80}BF_2N_5^+$ $[M]^+$ calcd: *m*/*z* 1447.6475; found: *m*/*z* 1447.9220.

Compound (16) The aza-BODIPY **13** (15.0 mg, 0.013 mmol) *N*-iodosuccinimide (8.7 mg, 0.038 mmol) were reacted in $CHCl_3$ (0.05 mL)/AcOH (0.13 mL) (3:1) mixture at room temperature for 10 h. The color of the reaction mixture changed from dark brown to blue, then it was washed with sodium thiosulfate and sodium bicarbonate and extracted with chloroform. The desired product was purified by silica gel column chromatography and eluted with 30% DCM/hexane. Evaporation of solvent mixture afforded aza-BODIPY **16** as blue green solid. Yield: 62% (32 mg). R_f = 0.19 (silica, DCM/hexane 1:2). ^{1}H NMR ($CDCl_3$, 500 MHz, δ ppm): 7.81-7.79 (m, 4H), 7.72 (d, *J* = 8.5 Hz, 4H), 7.64 (d, *J* = 8 Hz, 4H), 7.44-7.43 (m, 6H), 7.40 (d, *J* = 8 Hz, 4H), 7.13-7.07 (m, 22H), 7.08-7.04 (m, 12H). ^{13}C NMR ($CDCl_3$, 125 MHz, δ ppm): 158.62, 145.19, 143.72, 143.66, 143.63, 142.90, 141.49, 140.48, 137.99, 137.74, 134.81, 132.73, 131.92, 131.44, 131.37, 130.24, 130.13, 130.10, 129.64, 128.28, 127.83, 127.76, 127.67, 127.62, 126.88, 126.64, 126.57, 126.51, 126.28. ^{19}F NMR (470.4 MHz, $CDCl_3$, δ ppm): -130.46 (q, 2F). ^{11}B NMR (160 MHz, $CDCl_3$, δ ppm): 0.97 (t, 1B). MS (ESI-Q-TOF): $C_{84}H_{56}BF_2N_3I_2Na^+$ $[M]^+$ calcd: *m*/*z* 1432.2522; found: *m*/*z* 1431.2183.

References

[1] Wu D, Sedgwick AC, Gunnlaugsson T, Akkaya EU, Yoon J, James TD. Fluorescent Chemosensors: The past, present and future. Chem Soc Rev 2017;46(23):7105–23.

[2] Jiang Y, Pu K. Multimodal Biophotonics of Semiconducting Polymer Nanoparticles. Acc Chem Res 2018;51(8):1840–49.

[3] Chang YJ, Chow TJJ. Highly efficient red fluorescent dyes for organic light-emitting diodes. Mater Chem 2011;21(9):3091–99.

[4] Funabiki K, Mase H, Hibino A, Tanaka N, Mizuhata N, Sakuragi Y, Nakashima A, Yoshida, T, Kubota Y, Matsui M. Synthesis of a novel heptamethine-cyanine dye for use in near-infrared active dye-sensitized solar cells with porous zinc oxide prepared at low temperature. Energy Environ Sci 2011;4(6):2186–92.

[5] Fothergill SM, Joyce C, Xie F. Metal enhanced fluorescence biosensing: From ultra-violet towards second near-infrared window. Nanoscale 2018;10(45):20914–29.

[6] Vedamalai M, Kedaria D, Vasita R, Mori S, Gupta I. Design and synthesis of BODIPY-clickate based Hg^{2+} sensors: The effect of triazole binding mode with Hg2+ on signal transduction. Dalt Trans 2016;45(6):2700–08.

[7] Kesavan PE, Behera RN, Mori S, Gupta I. Carbazole Substituted BODIPYs: Synthesis, Computational, Electrochemical and DSSC Studies. J Fluoresc 2017; 27 (6), 2131–44.

[8] Kesavan PE, Das S, Lone MY, Jha PC, Mori S, Gupta I. Bridged bis-BODIPYs: Their synthesis, structures and properties. Dalt Trans 2015;44(39):17209–21.

[9] Mani V, Krishnakumar VG, Gupta S, Mori S, Gupta I. Synthesis and characterization of styryl-BODIPY derivatives for monitoring in vitro Tau aggregation. Sensors Actuators, B Chem 2017;244:673–83.

[10] Vedamalai M, Kedaria D, Vasita R, Gupta I. Oxidation of phenothiazine based fluorescent probe for hypochlorite and its application to live cell imaging. Sensors Actuators, B Chem 2018;263:137–42.

[11] Kolemen S, Akkaya EU. Reaction-based BODIPY probes for selective bio-imaging. Coord Chem Rev 2018;354:121–34.

[12] Boens N, Leen V, Dehaen W. Fluorescent indicators based on BODIPY. Chem Soc Rev 2012;41(3):1130–72.

[13] Vellanki L, Sharma R, Ravikanth M. Functionalized boron-dipyrromethenes and their applications. Reports in Organic Chemistry 2016;6:1-24.

[14] Mei J, Leung NLC, Kwok RTK, Lam JWY, Tang BZ. Aggregation-Induced Emission: Together We Shine, United We Soar!. Chem Rev 2015;115(21):11718–940.

[15] Li L, Wang L, Tang H, Cao D. A facile synthesis of novel near-infrared pyrrolopyrrole aza-BODIPY luminogens with aggregation-enhanced emission characteristics. Chem Commun 2017;53(59):8352–55.

[16] Li D, Qin W, Xu B, Qian J, Tang BZ. AIE Nanoparticles with High Stimulated Emission Depletion Efficiency and Photobleaching Resistance for Long-Term Super-Resolution Bioimaging. Adv Mater 2017;29(43):1–9.

[17] Tong H, Dong Y, Hong Y, Haussier M, Lam JWY, Sung HHY, Yu X, Sun J, Williams ID, Kwok HS, Tang BZ. Aggregation-induced emission: Effects of molecular structure, solid-state conformation, and morphological packing arrangement on light-emitting behaviors of diphenyldibenzofulvene derivatives. J Phys Chem C 2007;111 (5):2287–94.

[18] Peng L, Wang M, Zhang G, Zhang D, Zhu D. A fluorescence turn-on detection of cyanide in aqueous solution based on the aggregation-induced emission. Org Lett 2009;11(9):1943–46.

[19] Ding D, Li K, Liu B, Tang BZ. Bioprobes based on AIE fluorogens. Acc Chem Res 2013;46(11):2441–53.

[20] Gomez-Duran CFA, Hu R, Feng G, Li T, Bu F, Arseneault M, Liu B, Pena-Cabrera E, Tang BZ. Effect of AIE Substituents on the Fluorescence of Tetraphenylethene-Containing BODIPY Derivatives. ACS Appl Mater Interfaces 2015; 7(28):15168–76.

[21] Balsukuri N, Lone MY, Jha PC, Mori S, Gupta I. Structure, and Optical Studies of Donor-Acceptor-Type Near-Infrared (NIR) Aza-Boron-Dipyrromethene (BODIPY) Dyes. Chem An Asian J 2016;11(10)1572–87.

[22] Gobeze HB, Bandi V, D'Souza F. Bis(subphthalocyanine)–azaBODIPY triad for ultrafast photochemical processes Phys Chem Chem Phys, 2014;16(35):18720-28.

[23] Bandi V, Gobeze HB, Nesterov VN, Karr PA, D'Souza F. Phenothiazine–azaBODIPY–fullerene supramolecules: syntheses, structural characterization, and photochemical studies. Phys Chem Chem Phys 2014;16(46):25537-47.

[24] Pascal S, Bucher L, Desbois N, Bucher C, Andraud C, Gros CP. Synthesis, Electrochemistry and Photophysics of Aza-BODIPY Porphyrin Dyes. Chem Eur J 2016;22(14):4971-79.

[25] Kamkaew A, Burgess K. Aza-BODIPY dyes with enhanced hydrophilicity. Chem Commun 2015;51(53):10664–67.

[26] Murtagh J, Frimannsson DO, O'Shea DF. Azide conjugatable and pH responsive near-infrared fluorescent imaging probes. Org Lett 2009;11(23):5386–89.

[27] Guo S, Ma L, Zhao J, Kucukoz B, Karatay A, Hayvali M, Yaglioglu HG, Elmali. BODIPY triads triplet photosensitizers enhanced with intramolecular resonance energy transfer (RET): Broadband visible light absorption and application in photooxidation. Chem Sci 2014;5(2):489–500.

[28] Lu H, Mack J, Yang Y, Shen Z. Structural modification strategies for the rational design of red/NIR region BODIPYs. Chem Soc Rev 2014;43(13):4778–823.

[29] Shao J, Sun H, Guo H, Ji S, Zhao J, Wu W, Yuan X, Zhang C, James TD. A highly selective red-emitting FRET fluorescent molecular probe derived from BODIPY for the detection of cysteine and homocysteine: an experimental and theoretical study. Chem Sci 2012;3(4):1049-61.

[30] El-Khouly ME, Fukuzumi S, D'Souza, F. Photosynthetic Antenna–Reaction Center Mimicry by Using Boron Dipyrromethene Sensitizers. Chem Phys Chem 2014;15:30–47.

[31] Jiao L, Wu Y, Wang S, Hu X, Zhang P, Yu C, Cong K, Meng Q, Hao E, Vicente MGH. Accessing Near-Infrared-Absorbing BF_2-Azadipyrromethenes via a Push−Pull Effect J Org Chem 2014;79(4):1830−35.

[32] Wang M, Zhang G, Parvanova PB, Merriweather AN, Odom L, Barbosa D, Fronczek FR, Smith KM, Vicente MGH. Synthesis and Investigation of Linker-Free BODIPY–Gly Conjugates Substituted at the Boron Atom. Inorg Chem 2019;58(17):11614-21.

[33] Bandi V, El-Khouly ME, Nesterov VN, Karr PA, Fukuzumi S, D'Souza F. Self-Assembled via Metal−Ligand Coordination AzaBODIPY−Zinc Phthalocyanine and AzaBODIPY−Zinc Naphthalocyanine Conjugates: Synthesis, Structure, and Photoinduced Electron Transfer. J Phys Chem C 2013;117(11):5638−49.

[34] Bandi V, El-Khouly ME, Ohkubo K, Nesterov VN, Zandler ME, Fukuzumi S, D'Souza F. Bisdonor−azaBODIPY−Fullerene Supramolecules: Syntheses, Characterization, and Light-Induced Electron-Transfer Studies. J Phys Chem C 2014;118(5):2321−32.

[35] D'Souza F, Amin AN, El-Khouly ME, Subbaiyan NK, Zandler ME, Fukuzumi S. Control over Photoinduced Energy and Electron Transfer in Supramolecular Polyads of Covalently linked azaBODIPY-Bisporphyrin 'Molecular Clip' Hosting Fullerene. J Am Chem Soc 2012;134(1):654−64.

[36] Bandi V, D'Souza FP, Gobeze HB, D'Souza F. Multistep Energy and Electron Transfer in a "V-Configured" Supramolecular BODIPY–azaBODIPY–Fullerene Triad: Mimicry of Photosynthetic Antenna Reaction-Center Events. Chem Eur J 2015;21(6):2669-79.

[37] Bandi V, El-Khouly ME, Ohkubo K, Nesterov VN, Zandler ME, Fukuzumi S, D'Souza F. Excitation-Wavelength-Dependent, Ultrafast Photoinduced Electron Transfer in Bisferrocene/BF_2-Chelated-Azadipyrromethene/Fullerene Tetrads. Chem Eur J 2013;19(22):7221-30.

[38] Bandi V, Gobeze HB, D'Souza F. Ultrafast Photoinduced Electron Transfer and Charge Stabilization in Donor–Acceptor Dyads Capable of Harvesting Near-Infrared Light. Chem Eur J 2015;21(32):11483-94.

[39] Bandi V, D'Souza FP, Gobeze HB, D'Souza F. Competitive electron transfer in a novel, broad-band capturing, subphthalocyanine– AzaBODIPY–C60 supramolecular triad. Chem Commun 2016;52(3):579-81.

[40] Collini MA, Thomas MB, Bandi V, Karr PA, D'Souza F. Directly Attached Bisdonor-BF_2 Chelated Azadipyrromethene-Fullerene Tetrads for Promoting Ground and Excited State Charge Transfer. Chem Eur J 2017;23(18):4450-61.

[41] Bandi V, Gobeze HB, Karr PA, D'Souza F. Preferential Through-Space Charge Separation and Charge Recombination in V-Type Configured Porphyrin−azaBODIPY− Fullerene Supramolecular Triads. J Phys Chem C 2014;118(33):18969−82.

[42] Kumar S, Gobeze HB, Chatterjee T, D'Souza F, Ravikanth M. Directly Connected AzaBODIPY-BODIPY Dyad: Synthesis, Crystal Structure, and Ground- and Excited-State Interactions. J Phys Chem A 2015;119(30):8338–48.

[43] Su D, Oh J, Lee SC, Lim JM, Sahu S, Yu X, Kim D, Chang YT. Dark to light! A new strategy for large Stokes shift dyes: Coupling of a dark donor with tunable high quantum yield acceptors. Chem Sci 2014;5(12):4812–18.

[44] Şen E, Meral K, Atilgan S. From Dark to Light to Fluorescence Resonance Energy Transfer (FRET): Polarity-Sensitive Aggregation-Induced Emission (AIE)-Active Tetraphenylethene-Fused BODIPY Dyes with a Very Large Pseudo-Stokes Shift. Chem Eur J 2016;22(2):736–45.

[45] Lin L, Lin X, Guo H, Yang F. Diphenylacrylonitrile-connected BODIPY dyes: Fluorescence enhancement based on dark and AIE resonance energy transfer. Org Biomol Chem 2017;15(28):6006–13.

[46] Balsukuri N, Mori S, Gupta I. Donor acceptor type ferrocene substituted aza-BODIPYs: Synthesis, optical and electrochemical studies. J Porphyrins Phthalocyanines 2016;20(6):719–29.

[47] Yuan WZ, Lu P,Chen S, Lam JWY, Wang Z, Liu Y, Kwok HS, Yuguang M, Tang BZ. Changing the behavior of chromophores from aggregation-caused quenching to aggregation-induced emission: Development of highly efficient light emitters in the solid state. Adv Mater 2010;22(19):2159–63.

[48] Choi S, Bouffard J, Kim Y. Aggregation-induced emission enhancement of a meso-trifluoromethyl BODIPY via J-aggregation. Chem Sci 2014;5(2):751–55.

[49] Kasha M, Rawls HR, El-Bayoumi MA. The excitation model in molecular spectroscopy. Pure Appl Chem 1965;11:371–92.

[50] Shimizu S, Murayama A, Haruyama T, Iino T, Mori S, Furuta H, Kobayashi N. Benzo[c,d]indole-Containing Aza-BODIPY Dyes: Asymmetrization-Induced Solid-State Emission and Aggregation-Induced Emission Enhancement as New Properties of a Well-Known Chromophore. Chem Eur J 2015;21(37):12996–13003.

[51] Gorman A, Killoran J, O'Shea C , Kenna T, Gallagher WM, O'Shea DF. In vitro Demonstration of the Heavy-Atom Effect for Photodynamic Therapy. J Am Chem Soc 2004;126(34):10619-31.

[52] Balsukuri N, Boruah NJ, Kesavan PE, Gupta I. Near infra-red dyes based on pyrene aza-BODIPYs. New J Chem 2018;42(8):5875–88.

[53] Zou B, Liu H, Mack J, Wang S, Tian J, Lu H, Li Z, Shen Z. A new aza-BODIPY based NIR region colorimetric and fluorescent chemodosimeter for fluoride. RSC Adv 2014;4(96):53864–69.

[54] Qin W, Baruah M, Van der Auweraer M, De Schryver FC, Boens N. Photophysical Properties of Borondipyrromethene Analogues in Solution. J Phys Chem A. 2005;109(33):7371-84.

[55] Qian X, Xiao Y, Xu Y,Guo X, Qian J, Zhu W. "Alive" dyes as fluorescent sensors: Fluorophore, mechanism, receptor and images in living cells. Chem Commun 2010; 46(35):6418–36.

[56] Michael K. Characterization of electronic transitions in complex molecules. Discuss Faraday Soc 1950;9:14-19.

[57] Frisch MJ, Trucks GW, Schlegel HB, Scuseria GE, Robb MA, Cheeseman JR, Scalmani G, Barone V, Mennucci B, Petersson GA, Nakatsuji H, Caricato M, Li X, Hratchian HP, Izmaylov AF, Bloino J, Zheng G, Sonnenberg JL, Hada M, Ehara M, Toyota K, Fukuda R, Hasegawa J, Ishida M, Nakajima T, Honda Y, Kitao O, Nakai H, Vreven T, Montgomery JA, Peralta JE, Ogliaro F, Bearpark M, Heyd JJ, Brother E, Kudin KN, Staroverov VN, Kobayashi R, Normand J, Raghavachari K, Rendell A, Burant JC, Iyengar SS, Tomasi J, Cossi M, Rega N, Millam JM, Klene M, Knox JE, Cross JB, Bakken V, Adamo C, Jaramillo J, Gomperts R,

Stratmann RE, Yazyev O, Austin AJ, Cammi R, Pomelli C, Ochterski JW, Martin RL, Morokuma K, Zakrzewski VG, Voth GA, Salvador P, Dannenberg JJ, Dapprich S, Daniels AD, Farkas, Foresman JB, Ortiz JV, Cioslowski J, Fox DJ. Gaussian 09, Revis. B.01, Gaussian, Inc., Wallingford CT 2009:1–20.

[58] Adamo C, Barone V. Toward reliable density functional methods without adjustable parameters: The PBE0 model. J Chem Phys 1999, 110 (13), 6158–6170.

[59] Ernzerhof M, Scuseria GE. Assessment of the Perdew–Burke–Ernzerhof exchange-correlation functional. J Chem Phys 1999;110(11):5029-36.

[60] Hay PJ Wadt WR. Ab initio effective core potentials for molecular calculations. Potentials for K to Au including the outermost core orbitale. J Chem Phys 1985;82(1):299–310.

Highlights

- Donor-acceptor architectures consisting of tetraphenylethylene (TPE) and aza-BODIPY moieties are reported.
- Very efficient intramolecular energy transfer (80-91%) was observed from “donor TPE” to the acceptor “aza-BODIPY core”.
- Also, due to energy transfer process very large pseudo Stokes shifts (386-424 nm) were observed for such D-A systems.
- Femtosecond transient absorption studies supported energy transfer in the molecules.
- TD-DFT studies and single crystal X-ray technique are also used to get more insight about their spectral behaviour.

Authors state that, all co-authors have seen and approved the final version of the manuscript being submitted. Authors warrant that the article is our original work, which has not received prior publication and is not under consideration for publication elsewhere.

Declaration of interests

☒ The authors declare that they have no known competing financial interests or personal relationships that could have appeared to influence the work reported in this paper.

☒The authors declare the following financial interests/personal relationships which may be considered as potential competing interests:

Authors declare no conflict of interest.

Authors declare no financial interest.